Urban Eddy Covariance – The INFLUX Network

Jason P Horne[1], Scott J Richardson[1], Samantha L Murphy[1], Helen C Kenion[1], Bernd J Haupt[2], Benjamin J Ahlswede[1], Natasha L Miles[1], Kenneth J Davis[1, 2]

[1]Department of Meteorology and Atmospheric Science, The Pennsylvania State University, University Park, 16802, PA, USA

[2]Earth and Environmental Systems Institute, The Pennsylvania State University, University Park, 16802, PA, USA

Correspondence to: Kenneth J Davis (kjd10@psu.edu)

Abstract. The eddy covariance method is used by various disciplines to measure atmospheric fluxes of both vector and scalar quantities. One long-term, multi-site urban flux network experiment was the Indianapolis Flux Experiment (INFLUX), which successfully deployed and operated eddy covariance towers at eleven locations measuring fluxes from land cover types both in and surrounding the urban environment in Indianapolis, Indiana, USA. The data collected from this network of towers have been used to quantify urban greenhouse gas, energy, and momentum fluxes, assess the performance of numerical weather and carbon cycle models, and develop new analysis methods. This paper describes the available data associated with the INFLUX eddy covariance network, provides details of data processing and quality control, and outlines the site attributes to assist in data interpretation. For access to the various data products from the INFLUX eddy covariance work, please see the data availability section below.

Short summary. We present data from a network of instrumented towers in Indianapolis, used to study the exchange of heat, water vapor, and carbon dioxide between the surface and atmosphere in the city of Indianapolis, IN, USA. We explain what was measured, how we checked data quality, and why these observations improve our overall understanding of the urban environment.

1 Introduction

Eddy covariance (EC) is a method for quantifying atmospheric fluxes of mass, energy, and momentum. Near-surface EC measurements are commonly used to infer the exchange of these quantities between the Earth's surface and the atmosphere. Using EC, investigators can monitor a system with minimal disturbance over long periods, making it an attractive method for various disciplines (e.g., ecologists, meteorologists, hydrologists) (Baldocchi et al., 2001). The foundation of the technique is to sample the spectrum of turbulent eddies and the associated scalar constituents to calculate the covariance of the vertical wind component and the variable of interest. This covariance can be used to quantify the turbulent surface flux of a variable (vector or scalar) in many conditions (e.g. Yi et al. 2000). This method typically uses fast response (≥10Hz) instruments to measure the three-dimensional wind and various atmospheric scalars (e.g., CO_2, H_2O, temperature). A comprehensive description of the EC method can be found in Aubinet et al. (2012) and Burba (2013) or many micrometeorological-focused texts (Foken, 2008; Lee et al., 2004).

Urban environments are complex, challenging micrometeorological methods and theory that have been developed largely for horizontally homogeneous systems. In urban environments, heterogeneity (e.g., thermal, aerodynamic) is the norm rather than the exception. One approach to urban EC, however, is to require deployments in urban areas that are homogeneous for areas encompassing most of the EC flux footprint (i.e., upwind area measured by the EC system) (Turnbull et al., 2025). When possible, this greatly simplifies data interpretation.

A contrasting approach deploys EC flux measurements in heterogeneous settings and seeks to adapt our analysis methods and theories to the inherently heterogeneous nature of the urban environment. At least two issues emerge in this scenario. First, the EC flux measurements cannot be interpreted with respect to a single set of land surface characteristics. EC measurements collected in heterogeneous environments should be interpreted as a function of wind direction and atmospheric stability conditions, ideally with a flux footprint model (e.g., Horst and Weil, 1992; Kljun et al., 2015), and combined with data sets that can describe the urban landscape at a resolution that is finer than the flux footprint. Such data analysis is complicated by the fact that typical flux footprint models (e.g., Horst and Weil, 1992; Kljun et al., 2015) were developed for horizontally homogeneous environments and should therefore be used with caution in highly heterogeneous systems.

A second complication that must be considered is the formation of internal boundary layers and secondary circulations that can be created in heterogeneous environments (Bou-Zeid et al., 2020). These circulations can result in violations of common EC methodological assumptions, such as non-negligible horizontal flux divergence or mean advection (Feigenwinter et al., 2012). These flows violate the assumption of one-dimensional, vertical transport, which is typically used to infer surface-atmosphere exchange from EC flux measurements (Aubinet et al., 2012; Burba, 2013). Diagnosing the presence of such flows can be attempted, for example, with multi-level turbulent flux measurements (Yi et al., 2000). Yi et al. (2000) found only modest deviations from vertical-only transport in a highly heterogeneous forested region. In other locations, however, heterogeneity-induced secondary circulations have also been shown to impact EC measurements in arguably less complex settings (compared to an urban setting) like agricultural fields (Eder et al., 2015a) and deserts (Eder et al., 2015b), and have been linked to the lack of closure of the

surface energy balance endemic to EC flux measurements (Mauder et al., 2020). In summary, surface-atmosphere fluxes inferred from EC flux measurements collected in heterogeneous urban environments should also be treated with caution.

Mixed sources add complexity to the interpretation of urban EC flux measurements, as biological and anthropogenic factors are often interwoven. The combined impacts of anthropogenic and biogenic sources and sinks of CO_2 (Miller et al., 2020; Turnbull et al., 2019), sensible and latent heat (Ward et al.. 2022) and momentum (Kent et al., 2018) are measured by urban EC instruments. This complexity layers upon underlying mixtures of fluxes within natural (e.g., respiration and photosynthesis; evaporation and transpiration) and anthropogenic (vehicles and buildings; residential and industrial) systems.

None of these challenges, however, is new or unique to urban systems, and all have the potential to be addressed via ongoing research. Airborne EC has been conducted over heterogeneous flux footprints for decades (Desjardins et al., 1992; Oncley et al., 1997), and flux footprint decomposition methods have been employed for nearly as long (Schuepp et al., 1990; Mahrt et al., 2001). Footprint decomposition has been used with tower-based EC to study natural (Wang et al., 2006; Xu et al., 2017) and anthropogenic (Dennis et al., 2022; Wu et al., 2022) fluxes. Biological and anthropogenic CO_2 fluxes have been disaggregated in the urban environment using both statistical partitioning methods (Crawford and Christen 2015; Lee et al. 2021; Menzer and McFadden 2017) and tracer ratio methods (Ishidoya et al. 2020; Wu et al. 2022). Complex ecosystem flux sites (e.g., Davis et al., 2003) have served as a guide for flux upscaling studies (Wang et al., 2006; Xiao et al., 2014), and all AmeriFlux sites have been categorized according to their degree of heterogeneity (Chu et al., 2021). Lateral flow in low turbulence conditions has been recognized as a problem in all EC deployments (Barr et al., 2013). Landscape-scale secondary circulations have been investigated in agricultural (Kang et al., 2007) and forested landscapes (Butterworth et al., 2021). Given that urban environments are where over 55% (and rising) of the global population lives (Sun et al., 2020) and given the past successes in studying complex micrometeorological environments, we would like to stress the importance of understanding these complex systems and moving ahead with measurements that go beyond the classic homogeneous flux tower site.

Many efforts have successfully measured fluxes using EC in the urban environment (Biraud et al., 2021; Kotthaus and Grimmond, 2014; Menzer and McFadden, 2017; Vogt et al., 2006; Wu et al., 2022). Urban GHG emissions are a common focus of these efforts. Urban areas are responsible for 67-72% of anthropogenic CO_2 emissions globally (Lwasa et al., 2023). Many cities have pledged to reduce GHG emissions in this era of anthropogenic climate change. The EC method can directly measure GHG fluxes within the tower's footprint and reveal the urban metabolism. Liu et al., (2012) investigated spatial and temporal variability of CO_2 fluxes in the Beijing megacity using the EC method and found weekly (e.g., traffic volume) and seasonal (e.g., domestic heating) patterns in CO_2 fluxes. Crawford and Christen (2015) were able to disaggregate observed CO_2 fluxes into biogenic and anthropogenic sources by modeling various sources/sinks within the turbulent source area (i.e., flux footprint) of a residential area in Vancouver, Canada. Pawlak and Fortuniak (2016) assessed the temporal variability of CH_4 fluxes in a populated area of Łódź, Poland, and found the city's annual emissions (17.6 g m^{-2} $year^{-1}$) were comparable to surrounding natural sources like wetlands (18 g m^{-2} $year^{-1}$). Menzer and McFadden (2017) used statistical partitioning of CO_2 fluxes over a suburban neighborhood outside Saint Paul, Minnesota, (US-KUO: KUOM tower) to separate biogenic from anthropogenic sources.

Recent studies have employed an increasing number of urban EC measurements to study surface-atmosphere fluxes across multiple cities (Lipson et al., 2022; Nicolini et al., 2022; Papale et al., 2020). Nicolini et al. (2022) compared thirteen EC towers in eleven different European cities to assess the impacts of the COVID-19 lockdown on CO_2 emissions. They found a significant relationship between factors such as the lockdown stringency index and the relative CO2 flux change (i.e., before vs. during lockdown), demonstrating the value of EC measurements in detecting both long-term and short-term changes in CO_2 fluxes in real-time. The Urban-PLUMBER project (https://urban-plumber.github.io/) gathered measurements from twenty flux towers located all over the world, creating a dataset of urban EC measurements covering a spectrum of different climatic conditions and urban forms, and has used these data for urban land surface model evaluation (Lipson et al., 2022).

Most recently, intra-urban networks have begun to emerge. Multiple towers within and outside a single city enable a more detailed understanding of the urban system than could be achieved with a single flux tower. For example, Nicolini et al. (2022) were able to use paired towers within the same city (e.g., residential vs. non-residential) to infer qualitative information on the dominant CO_2 driver (e.g., vehicular, vegetation, etc.). Peters et al. (2011) showed the benefit of measuring turfgrass lawns using a short-stature (1.35 m) tower to help interpret evapotranspiration (ET) measurements made on the KUOM tall tower (40 m) in Saint Paul, Minnesota. In recent years there has been an expansion of urban EC in the United States through projects like the Indianapolis Flux Experiment (INFLUX, Davis et al., 2017), the Baltimore Social and Environmental Collaborative (BSEC), the Coastal Rural Atmospheric Gradient Experiment (CoURAGE, Davis et al., 2024), the Community Research on Climate and Urban Science (CROCUS, Raut et al., 2025), and the Southwest Urban Integrated Field Laboratory (SW-IFL, 2024).

INFLUX was a contribution to the urban greenhouse gas test beds program of the National Institute of Standards and Technology (Semerjian and Whetstone, 2021). This program endeavored to "improve emission measurement tools to better equip decision makers and mitigation managers with capabilities to chart progress in GHG emissions mitigation" (https://www.nist.gov/greenhouse-gas-measurements/urban-test-beds). The INFLUX project was the longest-running test bed in this program. Atmospheric inversions were the primary technological approach employed for urban GHG emissions estimates in the test bed program (Karion et al., 2023; Lauvaux et al., 2020; Yadav et al., 2023), given their ability to encompass emissions from the entirety of an urban area. Atmospheric inversions struggle, however, to infer the spatial structure of emissions within a city (e.g. Lauvaux et al., 2020). EC flux towers, long used to study fluxes at a spatial resolution more accessible to local-scale, process-based model evaluation, have been deployed in INFLUX to complement whole-city atmospheric inversions.

The INFLUX EC flux towers measured CO_2, H_2O, energy, and momentum fluxes in and around Indianapolis. The network included EC flux observations from eleven locations (Fig. 1), comprising over a decade and a half of observation site years (Table 1, Fig. 2). These tower locations range from agricultural sites in the croplands surrounding Indianapolis to towers in the cities' interior over turfgrass, suburban forests, residential areas, and heavily developed urban regions (Fig. 1). This multiplicity of flux sites was achieved by moving instrumentation from site to site as deemed necessary to sample the variability in fluxes in and around this urban landscape. A subset of the flux measurements (Table 1) have

been co-located with mole fraction observations (Richardson et al., 2017) from the INFLUX urban GHG testbed monitoring network (Miles et al., 2017a).

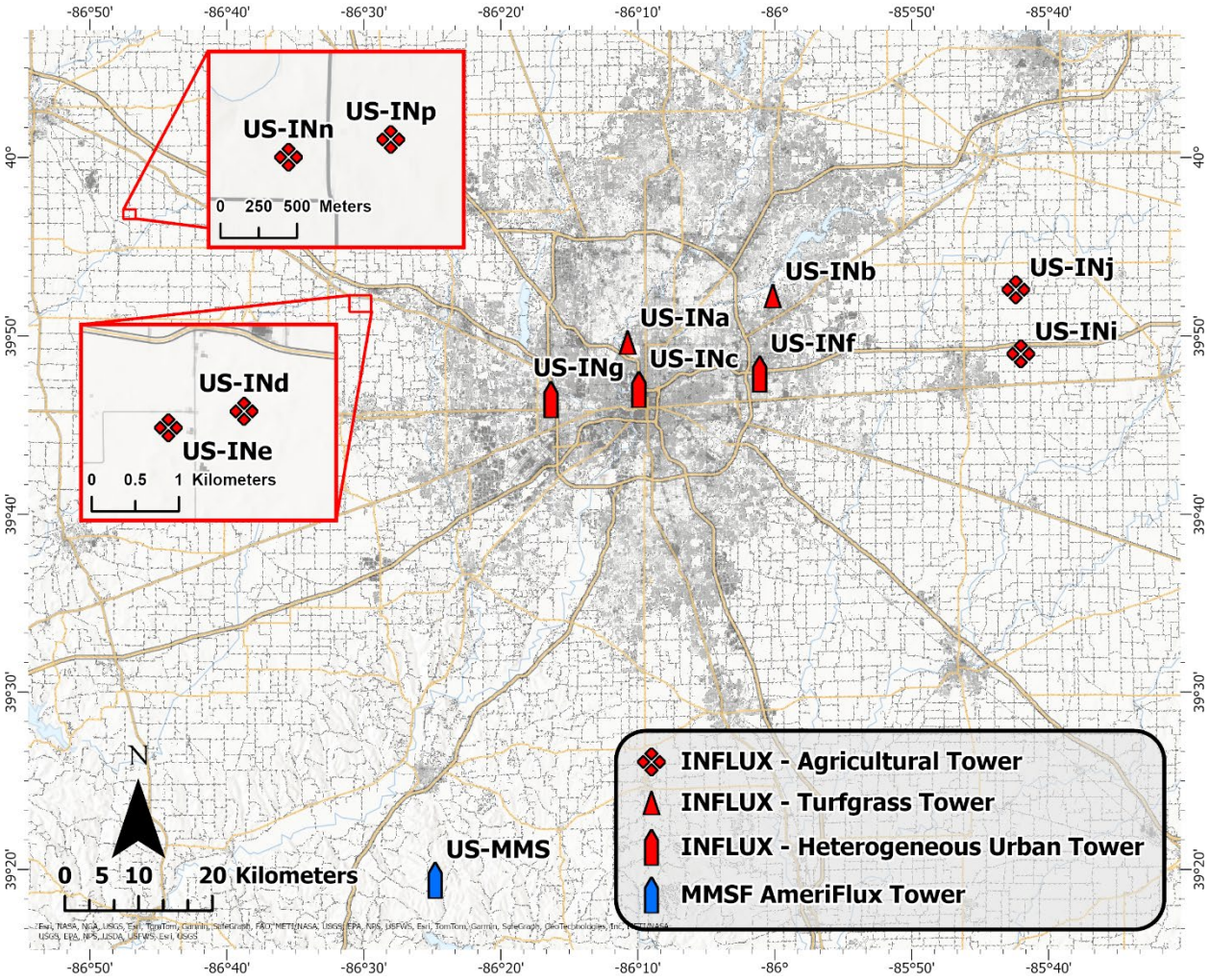

Figure 1. Locations of INFLUX eddy covariance towers in and around Indianapolis, IN. Specific flux tower site locations (i.e., latitude and longitude) are included in the site metadata file with the processed data files. The gray shading represents the 2023 impervious surface cover from the National Land Cover Database (doi.org/10.5066/P9JZ7AO3). Major roadways are depicted using orange lines, and waterways are shown in light blue. The Morgan-Monroe State Forest (MMSF) AmeriFlux tower is also included for spatial reference. Service layer credits go to City of Indianapolis, Marion County, Esri, TomTom, Garmin, SafeGraph, FAO, METI/NASA, USGS, EPA, NPS, USFWS, and GeoTechnologies Inc.

Table 1. Site identification in FLUXNET format, deployment period, and a short description of each site.

Site – Category	Time Start	Time End	Site Description
US-INa – Turfgrass	August 2017	April 2019	Pioneer Cemetery in Crown Hill Cemetery tower measured a minimally managed turfgrass lawn. Primarily cool-season C3 grass species.

US-INb – Turfgrass	November 2018	April 2019	The Fort Golf Resort tower measured a heavily managed turfgrass lawn. Primarily cool-season C3 grass species.
US-INc – Heterogeneous Urban	October 2020	May 2025	The downtown Indianapolis tower measured an urbanized, heterogeneous area and is also mole fraction site 03*.
US-INd – Agricultural	August 2017	November 2018	An agricultural tower near Pittsboro measured a mixture of corn and soy.
US-INe – Agricultural	September 2017	October 2020	An agricultural tower near Pittsboro measured corn (2018 and 2020) and soy (2019).
US-INf – Heterogeneous Urban	January 2013	November 2013	The tower at East 21st St measured a heterogeneous commercial and residential area, and also corresponds to the mole fraction site 02*.
US-INg – Heterogeneous Urban	April 2019	May 2025	Wayne Twp Comm tower measures a heterogeneous residential and commercial area and is also mole fraction site 07*.
US-INi – Agricultural	April 2019	May 2022	The agricultural tower measured soy (2019) and corn (2021). Located near mole fraction site 09*.
US-INj – Agricultural	May 2020	March 2023	The agricultural tower measured corn during both growing seasons (2020 and 2022). Located near mole fraction site 09*.
US-INn – Agricultural	April 2019	October 2021	Agricultural tower measured corn during 2019 and 2021. Located near mole fraction site 14*.
US-INp – Agricultural	May 2020	April 2021	The agricultural tower measured a mixture of corn and turfgrass in 2020. Located near mole fraction site 14*.

* Mole fraction towers and their numbers are described in Miles et al. (2017a).

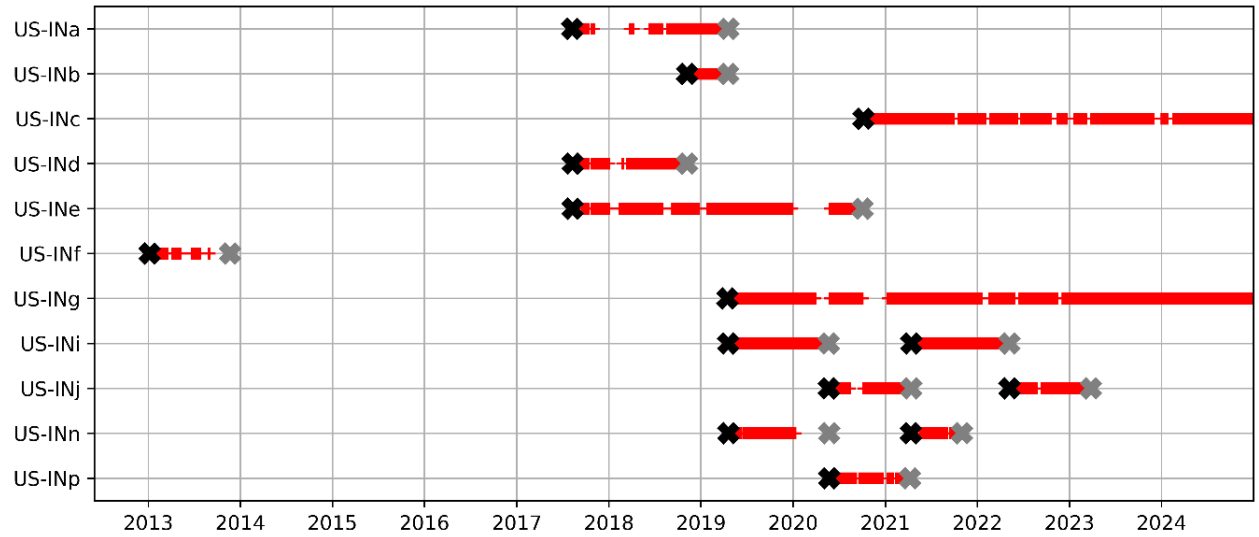

Figure 2: Data availability at each site through 2024. Each half-hour data point is indicated by a red "+", flux instrumentation deployment dates are indicated by black x's, and flux instrumentation decommissioning dates are indicated by gray x's. Any missing data between the deployment and decommissioning dates is due to power loss or instrument malfunction.

This paper documents the urban EC measurements undertaken as part of the INFLUX project. We discuss methods for quality-controlling the INFLUX EC measurements and describe the groups of EC flux sites within the INFLUX project (i.e., agricultural, turfgrass, and heterogeneous urban towers). We present the data processing required to interpret the data within this urban network and document the availability of data products.

2 INFLUX Eddy Covariance Tower Network

2.1 General Climate

The INFLUX project is based in and around Indianapolis, IN, USA. The city of Indianapolis and the surrounding area are on the boundary of two Köppen climate classifications, Dfa and Cfa (Kottek et al., 2006) at an elevation of approximately 220m above sea level. We reference data from the National Oceanic and Atmospheric Administration's (NOAA) National Centers for Environmental Information (NCEI) to provide averages for the period between 1991 and 2025. Indianapolis receives, on average, approximately 111 cm of liquid precipitation and 65 cm of snowfall (depth) annually. The annual average daily high and low temperatures are 17°C and 7°C, respectively.

2.2 Flux tower sites and site categories

The INFLUX flux towers can be subdivided into heterogeneous (US-INc, US-INg, US-INf) and homogeneous sites. Within the homogeneous grouping, we further subdivide the towers into agricultural (US-INd, US-INe, US-INi, US-INj, US-INn, US-INp) and turfgrass (US-INa, US-INb) categories. Each site is equipped with a sonic anemometer, either a Gill WindMaster (WindMaster, Gill Instruments, Lymington, UK) or CSAT3 (CSAT3, Campbell Scientific, Logan, UT, USA), and an infrared gas

analyzer (LI-7500DS or LI-7500A, LI-COR Biosciences, Lincoln, NE, USA) collecting data at 10Hz frequency (Table 2). The low-stature towers are also equipped with a temperature and humidity probe (HMP155, Vaisala Oyj, Vantaa, Finland), and a subset of them are equipped with photosynthetically active radiation (PAR) sensors (LI190R, LI-COR Biosciences, Lincoln, NE, USA) (Table 2). US-INc and US-INg were equipped with 4-way net radiometers (CNR4, Kipp and Zonen, Delftechpark, Netherlands) in October 2023 and March 2024, respectively. In addition to the INFLUX EC towers, the AmeriFlux Core Site US-MMS (Fig. 1), located in the Monroe-Morgan State Forest, is approximately seventy kilometers to the southwest of Indianapolis (Dragoni et al., 2011; Schmid et al., 2000).

Table 2. Measurement heights of deployed eddy covariance instruments and flux instruments for each site.

Site – Category	EC measurement height AGL	Infrared gas analyzer	Sonic anemometer	Temperature/ Humidity	PAR	Net Radiation	Arable
US-INa – Turfgrass	3 m	Licor LI-7500A	Campbell CSAT3	Vaisala HMP155	-	-	-
US-INb – Turfgrass	3 m	Licor LI-7500A	Campbell CSAT3	Vaisala HMP155	-	-	-
US-INc – Mixed Urban	43 m	Licor LI-7500A	Campbell CSAT3	-	-	Kipp & Zonen CNR4 (10/2023)	-
US-INd – Agricultural	3 m	Licor LI-7500A	Campbell CSAT3	Vaisala HMP155	-	-	-
US-INe – Agricultural	3 m	Licor LI-7500A	Campbell CSAT3	Vaisala HMP155	-	-	Yes
US-INf – Mixed Urban	30 m	Licor LI-7500A	Campbell CSAT3	-		-	-
US-ING – Mixed Urban	41 m	Licor LI-7500DS	Gill WindMaster	-	-	Kipp & Zonen CNR4 (03/2024)	-
US-INi – Agricultural	3 m	Licor LI-7500A	Campbell CSAT3	Vaisala HMP155	Licor LI190R	-	-
US-INj – Agricultural	3 m	Licor LI-7500A	Campbell CSAT3	Vaisala HMP155	Licor LI190R	-	Yes
US-INn – Agricultural	3 m	Licor LI-7500A	Campbell CSAT3	Vaisala HMP155	Licor LI190R	-	-
US-INp – Agricultural	3 m	Licor LI-7500A	Campbell CSAT3	Vaisala HMP155	-	-	Yes

2.3 Data acquisition and organization

The INFLUX EC instruments produce 10 Hz GHG data files, each containing thirty minutes of continuous data; 48 files per day. The GHG file is then transferred from the logger to a Linux server using the Secure Socket Shell (SSH) file transfer protocol. Each instrument has a unique incoming directory where the files are stored. Every night, a set of shell scripts checks to see if all 48 files have been delivered. Furthermore, every night, GHG files are copied to an archive while the data files are checked for (i) readability for further processing (occasionally some files are corrupt), (ii) monotonically time increase of recorded data (will be automatically corrected if possible), (iii) any non-ASCII characters which could cause problems during further scientific processing), (iv) incomplete data rows. Emails are automatically generated if any fault is recognized, while copies of the automatically modified and corrected data files are saved. Each step is captured in a log file. Missing data, errors, and file modifications due to errors trigger an email notification. These checks test file integrity and data completeness. Once the integrity tests are completed, the data is automatically processed and analyzed using EddyPro (LI-COR, 2021) and Python scripts. Graphics of the processed data (a two-week data window) are automatically updated online, allowing for manual monitoring of the incoming data and quick identification and resolution of issues. This allows researchers to quickly determine whether the instruments produce reasonable results or require immediate attention.

2.4 Flux processing and quality control

The complete time series of fluxes is calculated separately from the automatic processing script using a set of distinct post-processing steps and the EddyPro software package. For a comparison between EddyPro and other commonly used software (e.g., TK3 and eddy4R) when processing fluxes at heterogeneous urban flux towers, please see Lan et al. (2024). For every thirty minutes, we apply a block-averaging detrending (Foken, 2008; Lee et al., 2004) and planar fit coordinate rotation (Lee et al., 2004; Paw U et al., 2000; Wilczak et al., 2001). The Vickers and Mahrt (1997) despiking procedure is done before calculating fluxes, spikes are removed, and the number of spikes is reported. As the molar densities are measured by open-path sensors (LI-7500A or LI-7500DS), we apply the Webb, Pearman, and Leuning correction for density fluctuations (Lee and Massman, 2011; Paw U et al., 2000; Webb et al., 1980) following the iterative methodology employed in EddyPro. The cospectra are corrected (high and lowpass) via the analytical methods of Moncrieff et al. (1997), which is based on the methods of Moore (1986) using the similarity-based cospectral models from Kaimal et al. (1972). For each averaging period, using the methods of Vickers and Mahrt (1997), a set of flags is generated based on the high-frequency measurements. The deployment at US-INf was a preliminary effort that did not follow these same procedures. We employed a locally written EC code (Shi et al., 2013) that includes planar fit rotation and Vickers and Mahrt (1997) despiking algorithms. Due to differences in the data acquired for this system, we were unable to apply the data processing used for the remaining INFLUX towers. The US-INf data are described in more detail in Sarmiento et al. (2017) and Wu et al. (2022).

Flux data are flagged for violating an angle of attack test if >10% of the wind vectors exceed an attack angle of >|30º| for the averaging period. In the urban environment, the attack angle can be used to examine the impact of wake turbulence generated by roughness elements (RE) within the tower's footprint. For example, wind directions from the southwest (180-225°) of US-INc (Fig. 3) are flagged ≥ 30% of the time, detecting wake turbulence generated by a 30 m tall building 100 m southwest of the

tower. From these impacted wind directions, the measured fluxes are not within the inertial sublayer (i.e., the constant flux layer), where traditional EC assumptions are potentially valid.

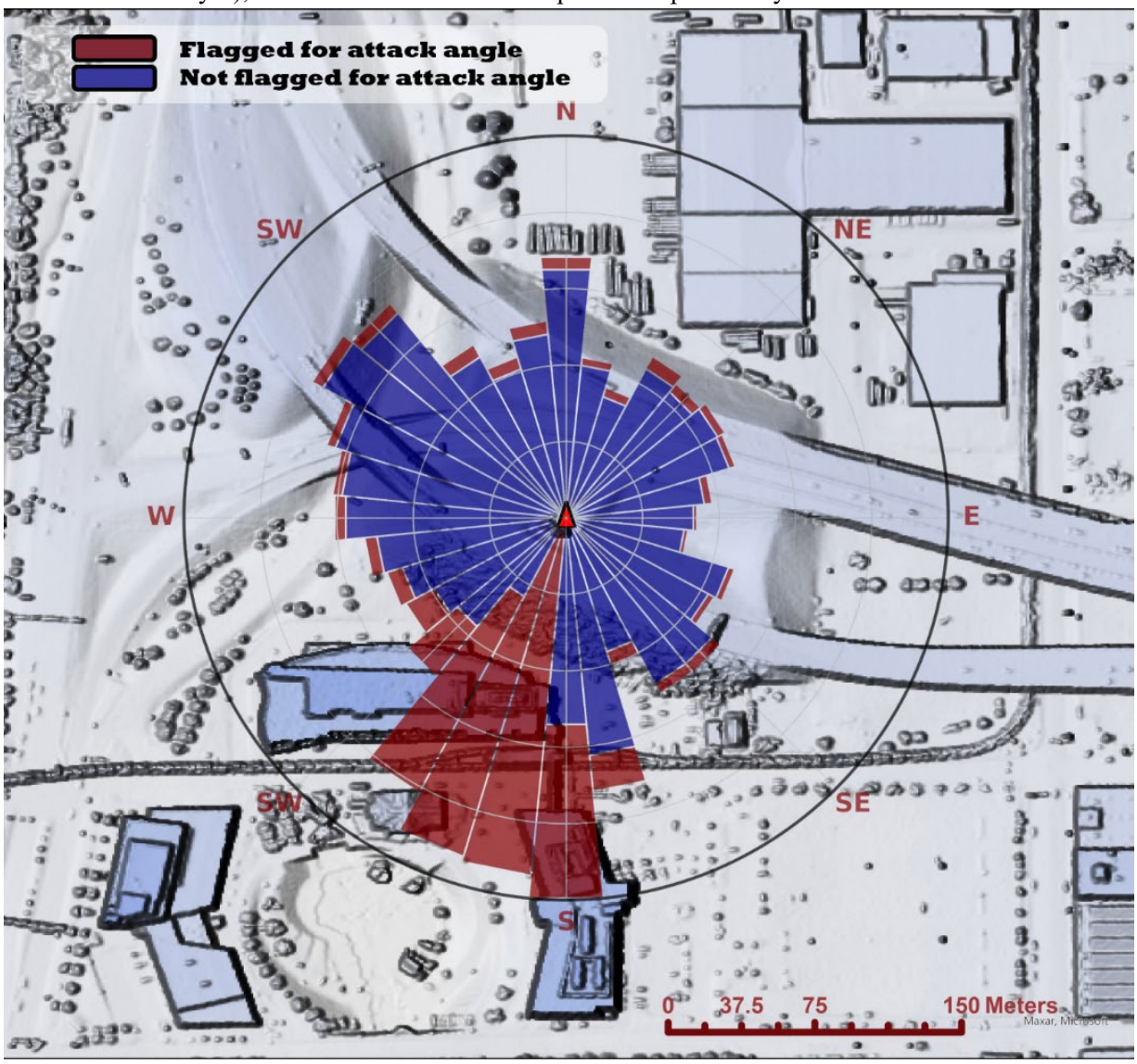

Figure 3. Percent of total data (i.e., all wind directions) flagged (radial) as a binary attack angle flagging (red/blue) vs. wind direction (angular) at US-INc (Oct 2020 – Jan 2023). Radial scales show 1.1, 2.2, 3.3, 4.4, and 5.6 percent of the total data moving from the inner to the outer ring, respectively. The red triangle represents the location of US-INc. The base map is a digital surface map generated using 2016 Indiana Statewide 3DEP LiDAR Data Products for Marion County (USDA, 2016). Service layer credits go to Maxar and Microsoft.

Fluxes are also flagged using a suite of quality control tests available through EddyPro, which are commonly used in EC research. Stationarity tests are conducted for each half-hour using the methodology of Foken and Wichura (1996) and Vickers and Mahrt (1997). Modeled integral turbulence characteristics from flux variance similarity theory are compared to measured variances of winds and scalars using the methods of Foken and Wichura (1996). Depending on the degree of nonstationarity and deviation from flux similarity theory, as determined by the Foken and Wichura (1996) tests, each averaging period is

assigned a value (1-9) based on the scheme of Mauder and Foken (2004). When comparing measurements made at the heterogeneous urban towers to similarity predictions, it is worth noting that aerodynamic parameters, such as displacement height, are often directionally dependent (Kent et al., 2018). Thus, the similarity-based relationship should scale differently depending on the wind direction. Subtle details, such as these, are not included in the current version of EddyPro, but the software's default flags, generated (as discussed here), can still guide users in interpreting the data.

For two agricultural sites, US-INn and US-INp, periods of the high-frequency data were lost, and only a version of the processed thirty-minute data using the default EddyPro settings was recovered. At US-INn, the period is from April 21, 2019, 00:00 UTC to January 10, 2020, 03:30 UTC, and at US-INp, it is from May 23, 2020, 21:30 UTC to December 22, 2020, 16:00 UTC. For these periods, a double rotation rather than a planar fit is used, and fluxes are flagged based on a simplified version of the 1-9 scheme, as outlined in the Spoleto agreement of 2004 for CarboEurope-IP, as described in Mauder and Foken (2004). These periods of missing high-frequency data have been combined with those where the high-frequency data is available, resulting in a mixture of flagging schemes and coordinate rotation in some columns.

After calculating half-hourly fluxes, additional screening methods generate flags based on periods with weak gas analyzer signals, extreme flux values, or inadequate mechanical mixing during nocturnal periods. The data are flagged if the signal strength reported by the gas analyzer for a half-hour period falls below the mean signal strength for a moving window of two weeks. Nighttime data (i.e., periods when the solar altitude is $\leq 0^{o}$) are flagged during low turbulent intensities based on the methods of Goulden et al. (1996). We acknowledge that the use of friction velocity filters in urban areas is still under question (Papale et al., 2022); a consensus has not been reached. We assert that this remains a valuable screening tool that we apply to this dataset. Finally, the flux data are flagged based on a threshold of N standard deviations from the mean, where N is a site-specific number chosen to keep flux magnitudes within geophysical limits.

We provide processed, half-hourly flux datasets for each of the eleven INFLUX sites through Penn State Data Commons and Ameriflux (See Section 3). Included with these data are metadata files with information on details such as flagging thresholds (e.g., friction velocity threshold) or site geographic coordinates. We do not remove data based on the generated flags for the data set available on Penn State Data Commons; instead, we leave the filtering decisions to the users. For most use cases, we do not recommend eliminating all points flagged using the quality control flags provided by the methods of Vickers and Mahrt (1997) and Mauder and Foken (2004), as a large proportion of physically reasonable data is flagged. We give an example of four different quality control flag combinations for CO_2, latent heat, sensible heat, and momentum fluxes using observations at Site US-INg in Fig. 4. The four quality control flag combinations for each of these fluxes are summarized in Table 3. We recommended at minimum filtering the data according to friction velocity and CO_2 flux standard deviation flags for analysis of CO_2 fluxes, sensible heat standard deviations flags for analysis of sensible heat fluxes, latent heat standard deviation flags for analysis of latent heat fluxes, and removing wind directions from which the measurement is impact by distortion due to the tower (for Site US-INg, observations from wind directions 30-135° should be removed) for momentum fluxes (Set 1 in Table 3). From wind directions where the towers distort the flow, we do not observe a clear impact on scalar fluxes; thus, we leave the decision for removal to the data user. To remove additional outlier points, we suggest filtering by Sets 2 or

3 (Table 3) as shown in Fig. 4b and Fig. 4c for CO_2 fluxes, Fig. 4f and Fig. 4g for sensible heat fluxes, Fig. 4j and Fig. 4k for latent heat fluxes, and Fig. 4n and Fig. 4o for momentum fluxes. Given the significant reduction of overall data points, we do not suggest the flagging combination of Set 4, as shown in Fig. 4d, h, l, and p, unless the application of the data requires the strictest turbulence screening, which is appropriate only if the most idealized conditions for EC flux measurements are needed. At the heterogeneous urban flux towers (US-INc and US-INg), we recommend not removing scalar flux data based on the Vickers and Mahrt (1997) higher-moment statistics (i.e., skewness and kurtosis), as these flags commonly target realistic data at these sites (Järvi et al., 2018). This is due to the spatial and temporal heterogeneity of the urban environment, which can cause the distribution of high-frequency scalar measurements for a single period often to exceed the default skewness or kurtosis thresholds in EddyPro.

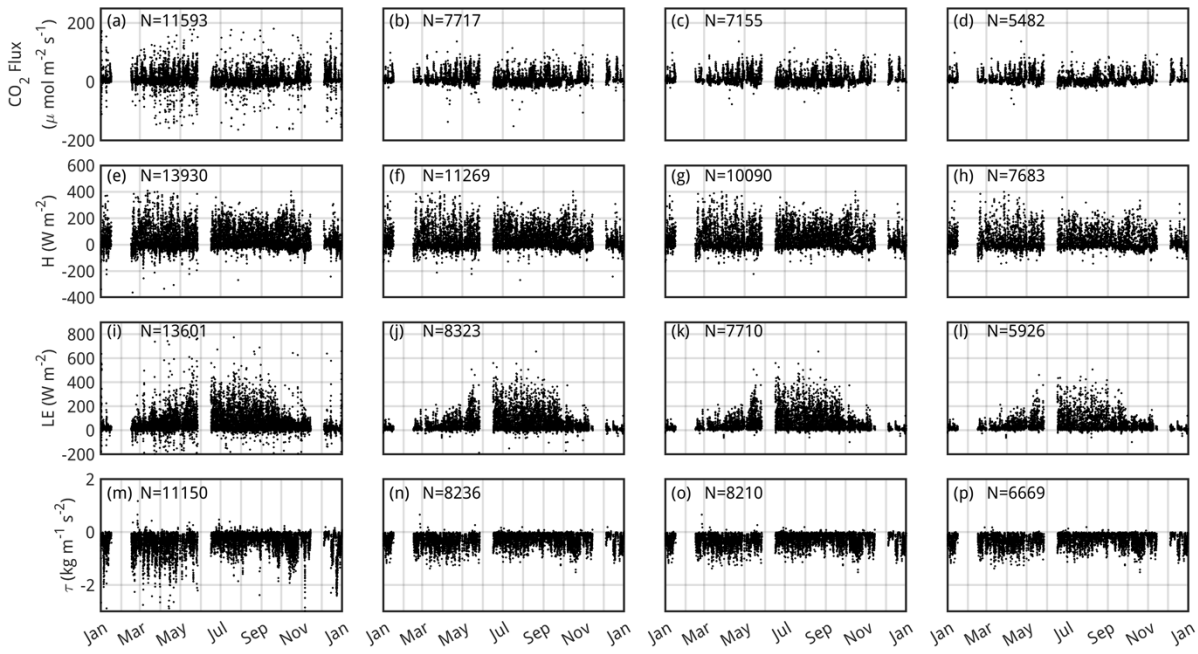

Figure 4. CO_2 fluxes (panels (a)-(d)), sensible heat fluxes (H) (panels (e)-(h)), latent heat fluxes (LE) (panels (i)-(l)), and momentum fluxes (τ) (panels (m)-(p)) at Site US-INg for 2022 with different quality control flags applied. From left to right, the filtering sets 1, 2, 3, and 4 (see Table 3 for full set descriptions) are shown for each of the fluxes, representing a range of filtering choices from least to most stringent. The number of points remaining in the dataset after removing quality control flags is indicated on each panel. With no filtering applied, there are 13,779 CO_2 flux data points, 13,969 sensible heat data points, 13,697 latent heat flux data points, and 13,969 momentum flux data points. For filtering Sets 1, 2, 3, and 4, respectively, 84.1%, 56.0%, 51.9%, and 39.7% of the total CO_2 flux data are preserved, 99.7%, 80.6%, 72.2%, and 55.0% of sensible heat flux data are preserved, 99.2%, 60.7%, 56.2%, and 43.2% of latent heat flux data are preserved, and 79.8%, 58.9%, 58.7% and 47.7% of momentum flux data are preserved.

Table 3: Description of quality control flag combinations considered for CO_2, sensible heat (H), latent heat (LE), and momentum (τ) fluxes. The hard flag is abbreviated as 'hf' in the table.

Flux	Set 1	Set 2	Set 3	Set 4

CO_2	Friction velocity	Friction velocity	Friction velocity	Friction velocity
	CO_2 flux standard deviation	CO_2 flux standard deviation	CO_2 flux standard deviation	CO_2 flux standard deviation
		Spike hf w	Spike hf w	Spike hf w
		Amplitude resolution hf w	Amplitude resolution hf w	Amplitude resolution hf w
		Drop out hf w	Drop out hf w	Drop out hf w
		Absolute limits hf w	Absolute limits hf w	Absolute limits hf w
		Discontinuities hf w	Discontinuities hf w	Skewness and kurtosis hf w
		Spike hf CO_2	Spike hf CO_2	Discontinuities hf w
		Amplitude resolution hf CO_2	Amplitude resolution hf CO_2	Spike hf CO_2
		Drop out hf CO_2	Drop out hf CO_2	Amplitude resolution hf CO_2
		Absolute limits hf CO_2	Absolute limits hf CO_2	Drop out hf CO_2
		Discontinuities hf CO_2	Discontinuities hf CO_2	Absolute limits hf CO_2
		Signal strength	Signal strength	Discontinuities hf CO_2
			CO_2 QC greater than 5	Signal strength
				CO_2 QC greater than 5
				Attack angle hf
				Nonsteady wind hf
H	H standard deviation	H standard deviation	H standard deviation	H standard deviation
		Spike hf w	Spike hf w	Spike hf w
		Amplitude resolution hf w	Amplitude resolution hf w	Amplitude resolution hf w
		Drop out hf w	Drop out hf w	Drop out hf w
		Absolute limits hf w	Absolute limits hf w	Absolute limits hf w
		Discontinuities hf w	Discontinuities hf w	Skewness and kurtosis hf w
			H QC greater than 5	Discontinuities hf w
				H QC greater than 5
				Attack angle hf
				Nonsteady wind hf
LE	H_2O flux standard deviation	H_2O flux standard deviation	H_2O flux standard deviation	H_2O flux standard deviation
		Spike hf w	Spike hf w	Spike hf w
		Amplitude resolution hf w	Amplitude resolution hf w	Amplitude resolution hf w
		Drop out hf w	Drop out hf w	Drop out hf w
		Absolute limits hf w	Absolute limits hf w	Absolute limits hf w
		Discontinuities hf w	Discontinuities hf w	Skewness and kurtosis hf w
		Spike hf H_2O	Spike hf H_2O	Discontinuities hf w
		Amplitude resolution hf H_2O	Amplitude resolution hf H_2O	Spike hf H_2O

		Drop out hf H_2O Absolute limits hf H_2O Skewness and kurtosis hf H_2O Signal strength	Drop out hf H_2O Absolute limits hf H_2O Skewness and kurtosis hf H_2O Signal strength LE QC greater than 5	Amplitude resolution hf H_2O Drop out hf H_2O Absolute limits hf H_2O Skewness and kurtosis hf H_2O Signal strength LE QC greater than 5 Attack angle hf Nonsteady wind hf
τ	Wind directions impacted by tower distortion	Wind directions impacted by tower distortion Spike hf w Amplitude resolution hf w Drop out hf w Absolute limits hf w Discontinuities hf w Spike hf v Amplitude resolution hf v Drop out hf v Absolute limits hf v Discontinuities hf v Spike hf u Amplitude resolution hf u Drop out hf u Absolute limits hf u Discontinuities hf u Attack angle hf	Wind directions impacted by tower distortion Spike hf w Amplitude resolution hf w Drop out hf w Absolute limits hf w Discontinuities hf w Spike hf v Amplitude resolution hf v Drop out hf v Absolute limits hf v Discontinuities hf v Spike hf u Amplitude resolution hf u Drop out hf u Absolute limits hf u Discontinuities hf u QC τ greater than 5 Attack angle hf	Wind directions impacted by tower distortion Spike hf w Amplitude resolution hf w Drop out hf w Absolute limits hf w Skewness and kurtosis hf w Discontinuities hf w Spike hf v Amplitude resolution hf v Drop out hf v Absolute limits hf v Skewness and kurtosis hf v Discontinuities hf v Spike hf u Amplitude resolution hf u Drop out hf u Absolute limits hf u Skewness and kurtosis hf u Discontinuities hf u QC τ greater than 5 Attack angle hf Nonsteady wind hf

2.5 Agricultural Sites

Understanding the boundary layer dynamics and CO_2 fluxes surrounding a city is important for understanding measurements collected within the city. The area surrounding Indianapolis is mainly composed of agricultural fields planted with a rotation of corn and soybeans. We deployed short-stature (~3-m AGL) flux towers at six locations in agricultural fields within 30-60 km of downtown Indianapolis (Fig. 1). The instrumentation for the agricultural sites was, in most cases, relocated annually to sample a variety of fields (specifically US-INd, US-INe, US-INn, US-INp). Each location was given a different site key. We collected data at the six agricultural sites for eleven growing seasons (Fig. 5).

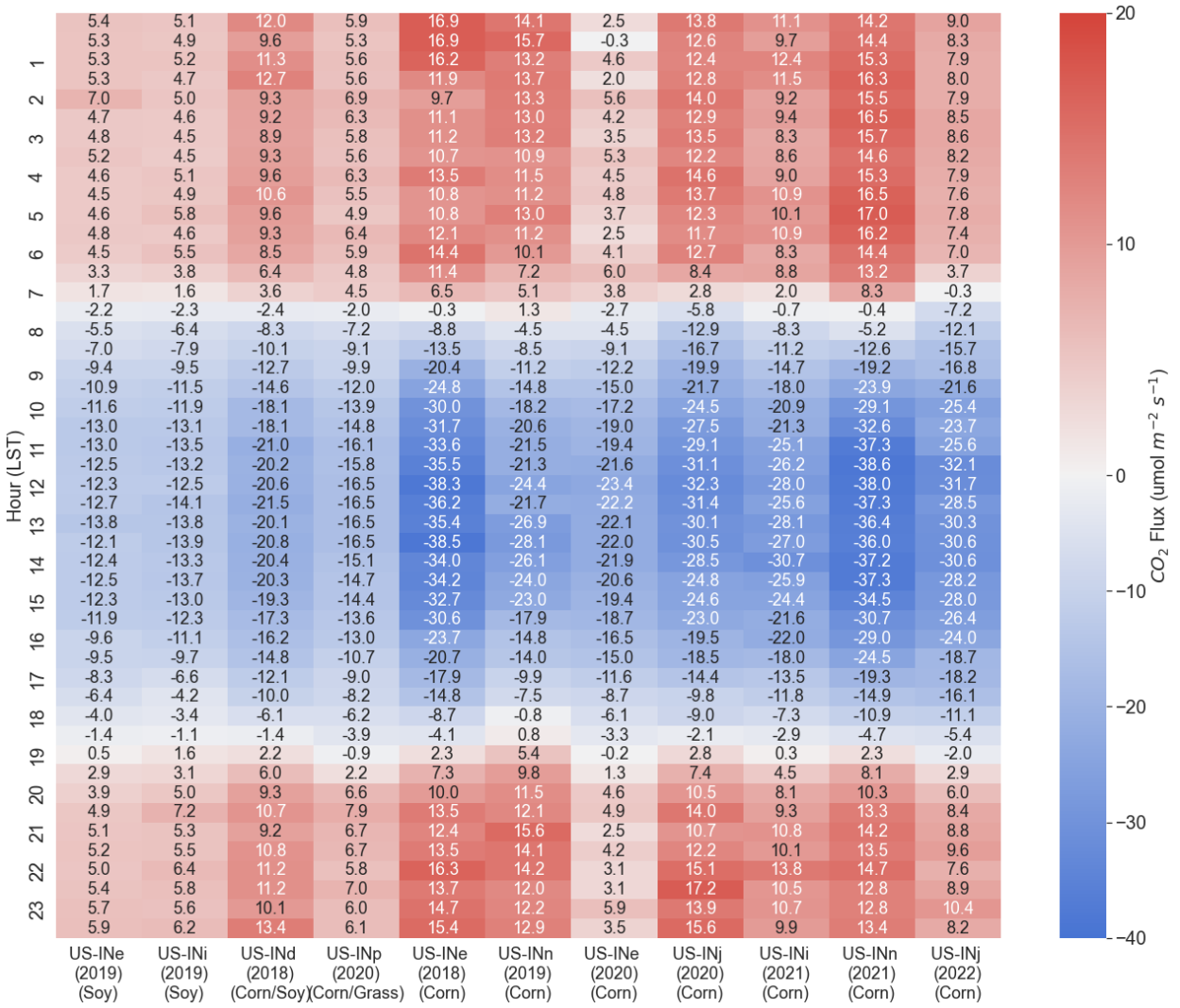

Figure 5. The average summer (JJA) diel cycle of CO_2 fluxes for each agriculture site-year. Each column is also labeled with the surrounding vegetation. The numbers indicate the average value for each half-hour flux corresponding to the underlying color. Text color is for visual purposes only.

Flux footprint analyses are used to identify averaging periods when these agricultural towers may have been strongly influenced by vegetation other than the crops to be sampled. These conditions arise from the practical need to place the flux towers close to, but not directly within, the actively managed crop fields. The fractional coverage of the agricultural crop of interest (corn or soybean) within the estimated tower footprint was calculated for each agricultural flux site in the INFLUX network. The calculated fractional coverage values allow a data user to select thresholds for which they would consider

the half-hourly flux value representative of the vegetation of interest. The Flux Footprint Prediction (FFP) model, developed by Kljun et al. (2015), is utilized to calculate the vegetation fraction for each point in the data record. Atmospheric boundary layer heights for input into the FFP come from ERA5 reanalysis (Hersbach et al., 2023). Imagery from Google Earth and ArcGIS Pro software is used to visually select areas covered with the vegetation of interest. Areas with the vegetation type of interest are assigned a value of one, while other areas are assigned a value of zero. For all half hours during which the required input data are available, the FFP climatology function simulates footprints at a 1 m grid spacing for a 501 m by 501 m domain. The site map distinguishing landcover types and the footprint estimate is multiplied to obtain a gridded map representing only the footprint attributable to the vegetation of interest. For every possible half hour, two values are computed using the predicted footprints: a value representing the footprint attributable to the vegetation of interest and a value for the total footprint. The former is calculated by summing over the footprint attributable to the vegetation of interest, and the latter by summing the footprint over the entire domain. The ratio of these values represents the fraction of the footprint attributable to the vegetation of interest.

The agricultural EC measurements have been used to evaluate the background conditions for the city. Murphy et al. (2025) evaluated the accuracy and precision of a simple carbon flux model used to describe ecosystem CO_2 fluxes surrounding the city. Ongoing work is evaluating the latent and sensible heat fluxes simulated by numerical weather prediction (NWP) models. These models are necessary for conducting urban climate and GHG inversion studies.

2.6 Turfgrass Sites

Turfgrass is a common urban land cover (Milesi et al., 2005). Only a handful of towers have previously been deployed to measure turfgrass lawns (i.e., mixed species low-stature vegetation often artificially managed through irrigation, fertilization, and/or mowing) (Ng et al., 2015; Pahari et al., 2018; Pérez-Ruiz et al., 2020; Peters and McFadden, 2012) despite these lawns being an abundant vegetative community in urban areas (Horne et al., 2025). We deployed two flux towers (US-INa and US-INb) to monitor turfgrass lawns. The two INFLUX turfgrass towers captured different levels of management intensity. US-INa measured fluxes over a cemetery lawn (Fig. 6) with lower intensity management (i.e., infrequent mowing, no fertilization, and no irrigation), and US-INb measured fluxes over a golf course (i.e., frequent mowing, fertilization, and irrigation). These towers were of low stature and sited to minimize contributions to the flux footprint from anything other than turfgrass. We have used the CO_2 flux data from these two turfgrass towers to evaluate the Vegetation Photosynthesis and Respiration Model (VPRM) performance at reproducing seasonal turfgrass fluxes, finding that these lawns require a unique representation in the VPRM (Horne et al., 2025). These towers are also being used in ongoing analyses of the sensible and latent heat fluxes in NWP models.

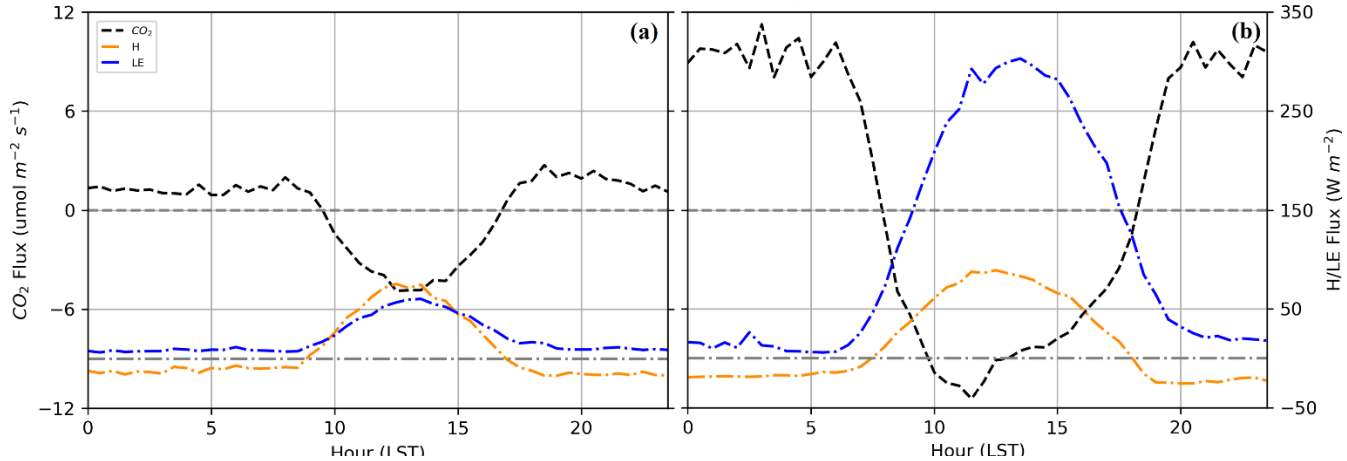

Figure 6. The average winter (DJF) (a) and summer (JJA) (b) diel cycle of latent heat (LE), sensible heat (H), and CO_2 fluxes for US-INa (cemetery lawn). Data for averaging are taken from the periods over the site deployment (Aug 2017 – April 2019). The dashed and dashed-dot horizontal lines indicate zero crossings for the CO_2 or sensible and latent heat flux, respectively.

2.7 Heterogeneous Footprint (Mixed) Urban Flux Towers

Three communications towers with EC instrumentation at 30 to 43 m AGL were instrumented to measure fluxes from the complex, mixed land cover typical of urban environments. These higher-altitude measurements are necessary to measure fluxes above the trees and buildings commonly found throughout the metropolitan area. As mentioned, these towers host flux instrumentation and mole fraction measurements that are part of the INFLUX urban GHG testbed monitoring network (Miles et al., 2017a; Davis et al., 2017). In addition, publicly available high-resolution data, although not included here, are available and can complement specific investigations, aiding users in interpreting measurements. Footprint climatologies generated using the Kljun et al. (2015) FFP model for the INFLUX mixed urban flux towers are shown in Figs. 7. We include footprint climatologies for these sites alone to show the level of heterogeneity at each site and the estimated area measured by these towers. These footprint climatologies guide our characterization of the regions sampled by these towers. We describe broad characteristics of the urban landscapes in their flux footprints following the example of the Urban-PLUMBER project (https://urban-plumber.github.io/, Lipson et al., 2022). Table 4 provides metadata for the area surrounding the three heterogeneous urban flux towers (US-INc, US-INf, US-INg). In Table 4, values for roughness length (z_0) and displacement height (z_d) are provided. These length scales are simultaneously fitted using the logarithmic wind profile and isolating measurement periods during near-neutral conditions ($|z/L| < 0.05$, where z is the height of the EC measurement and L is the measured Obukhov length), where the tower frame does not impact the measurement. These provided z_d and z_0 values serve as a reasonable first-order estimate for use in a flux footprint model. It should be noted that

Table 4. Metadata for the surrounding land cover at the three heterogeneous flux towers. We include values of roughness length (z_0) and displacement height (z_d) for each of the towers. The domain is 4 km^2 centered around the respective tower and separated into quadrants NE [0-90°), SE [90-180°), SW [180-270°), and NW [270-360°) to capture heterogeneity surrounding the tower. Data for percent impervious

and canopy fractions come from the National Land Cover Database (NLCD) using data for 2021 (US-INc and US-ING) and 2013 (US-INf) (doi.org/10.5066/P9JZ7AO3). LiDAR data used to estimate roughness elements (RE) (buildings and trees ≥2m) characteristics comes from the 2016 Indiana Statewide 3DEP LiDAR Data Products for Marion County (USDA, 2016). Roughness element density is the ratio of surface area occupied by REs to total surface area (i.e., planar area index).

Site	Quadrant	Local Climate Zone (LCZ)	Percent impervious (%)	Percent tree canopy cover (%)	Planar density ($m^2 m^{-2}$)	Mean RE height (m)	RE standard deviation (m)	Maximum RE height (m)
US-INc (43m AGL)	NE	LCZ 8 (Large low-rise)	86	1	0.29	10.6	8.9	53
z_0: 0.33m	SE	LCZ 8 (Large low-rise)	85	2	0.32	9.4	8.7	57
z_d: 2m	SW	LCZ 6 (Open low-rise)	69	5	0.33	6.9	5.2	36
	NW	LCZ 6 (Open low-rise)	58	6	0.23	5.8	3.7	25
US-INf (30m AGL)	NE	LCZ 8_{Bc} (Large low-rise with scattered trees)	67	4	0.27	6.1	2.7	30
z_0: 0.17m	SE	LCZ 6 (Open low-rise)	41	12	0.31	5.1	2.4	25
z_d: 4m	SW	LCZ 6 (Open low-rise)	41	14	0.43	5.2	2.4	31
	NW	LCZ 6 (Open low-rise)	49	11	0.35	5	2.1	23
US-ING (41m AGL)	NE	LCZ 8_B (Large low-rise with scattered trees)	64	4	0.19	5.4	2.1	25
z_0: 0.11m	SE	LCZ 6 (Open low-rise)	50	6	0.22	5.4	2.2	22
z_d: 1.5m	SW	LCZ 6 (Open low-rise)	35	12	0.33	5.4	2.6	34
	NW	LCZ 6 (Open low-rise)	42	15	0.33	4.9	2.2	22

data from these towers have been employed in multiple previous studies. Wu et al. (2022) demonstrated a method of disaggregation using INFLUX EC data and mole fraction measurement profiles available at the three INFLUX mixed urban flux towers (Richardson et al., 2017; Miles et al., 2017a), as well as tracer

ratio methods. This methodology estimates the fossil fuel component of the CO_2 flux by combining carbon monoxide (CO) flux estimates with measurements of the CO to CO_2 flux ratio from fossil fuel combustion (Turnbull et al., 2015). The biogenic CO_2 flux is then determined by subtracting the fossil fuel flux from the total CO_2 flux measured via EC. Vogel et al. (2024) applied this methodology to the flux record from US-INg to study changes in emissions caused by the COVID-19 lockdown. Both Wu et al. (2022) and Vogel et al. (2024) employed flux footprint and tracer decomposition methods in conjunction to compare the EC measurements with the Hestia urban emissions inventory (Gurney et al., 2012). Kenion et al. (2024) used US-INc EC flux data to demonstrate our ability to infer local-scale urban GHG fluxes using flux-gradient and flux-variance methods. These approaches can be applied to mole fraction measurement sites that are relatively abundant across the NIST urban test beds and other urban GHG mole fraction monitoring programs.

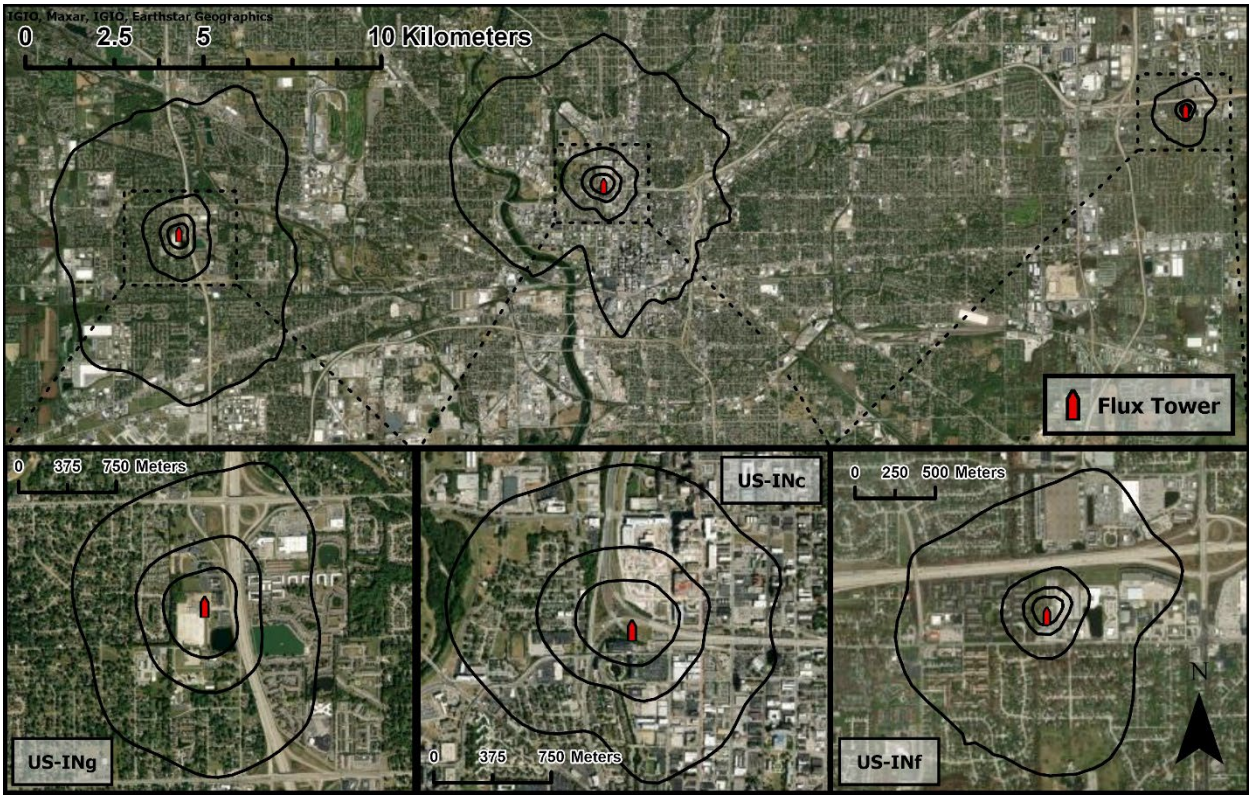

Figure 7. Flux footprint climatologies for all three heterogeneous urban flux towers are shown. Footprint climatologies are created using the Kljun et al. (2015) flux footprint prediction (FFP) model and available data from 2022 (US-INc and US-INg) or 2013 (US-INf). Boundary layer height data for FFP are provided by ERA5 reanalysis. The outermost climatology boundary represents 90% of the area, and extents moving towards the respective tower represent a 20% decrease in climatological area (i.e., 70%, 50%, 30%). Wind directions impacted by the building wake (Fig. 2) at US-INc are removed. Zoomed-in maps of the area around each tower are provided, with their extent shown by the dashed outlines on the upper plot. Service layer credits go to Earthstar Geographics, IGIO, and Maxar.

Two mixed urban flux towers, US-INf and US-INg, can each be interpreted as two distinct flux tower sites. We describe these differences in terms of building and vegetation cover (Table 4) and local climate zones (LCZ) (Stewart and Oke, 2012). The EC instruments at US-INg, for example, are set between a highway (LCZ E – Bare rock or paved) and commercial buildings (LCZ 8_B – Large low-rise with

scattered trees) to the east and a forested residential neighborhood (LCZ 6 - Open low-rise) to the west. The two sectors exhibit dissimilar diel patterns of CO_2 fluxes (Fig. 8). To the west, we observe a photosynthetic drawdown from the suburban forest during the growing season. To the east, we can observe two distinct peaks in net emissions, corresponding to morning and evening rush-hour traffic (Vogel et al., 2024). We suggest interpreting these sectors independently, potentially thought of as two distinct flux towers. Similarly, the footprint at US-INf is divided roughly into northerly and southerly sectors (Table 4), with highway and commercial areas to the north and residences to the south. Multiple INFLUX studies (Vogel et al., 2024; Kenion et al., 2024; Wu et al., 2022) have shown that the results are highly interpretable using this simple wind direction interpretation.

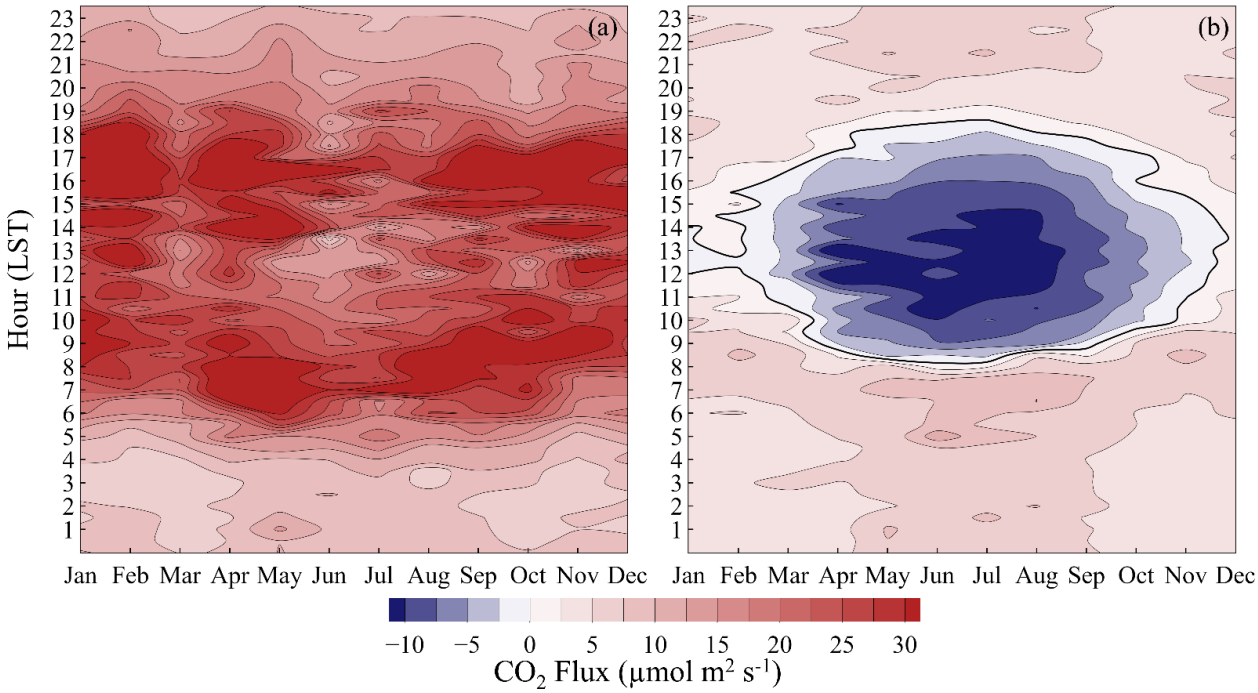

Figure 8. Isopleths of measured CO_2 flux at US-INg (April 2019 - January 2023) as a function of time of year (x-axis) and time of day (y-axis) for a) westerly wind directions (180 - 360º] and b) easterly wind directions (0 - 180º]. Positive values indicate net emissions of CO_2; negative values indicate a net uptake of CO_2.

We have not divided the flux data from US-INf and US-INg into two distinct records, nor have we posted flux footprint data sets to accompany each flux tower. However, the flux tower records contain all the data needed to subdivide the datasets and produce flux footprints, except for the atmospheric boundary layer height, which can be obtained from reanalysis products such as ERA5 (Hersbach et al., 2023). We note that urban systems frequently violate the assumptions implicit in the surface layer similarity theory and, consequently, the current flux footprint models (e.g., homogeneous turbulence forcing within the flux footprint). We, along with others, such as Feigenwinter et al. (2012), argue that existing footprint models (e.g., Kljun et al., 2015) remain quite helpful in interpreting these datasets. However, more research into the sensitivity of these models to complex urban systems is warranted.

3 Data availability

Unprocessed 10Hz data and processed INFLUX data are available on Penn State Data Commons (Table 5). This version contains all the processed data with flagging, but no data has been removed based on flagging. This processed data also included a metadata file describing the naming convention of variables and flagging. Data from all agricultural sites includes calculated fractional coverage and data collected using the Arable sensors on-site.

Table 5. Citations for each INFLUX tower. The raw data collected directly from the instruments, a processed version of the data available on Ameriflux, and a processed version with no flagged data removed are available through Penn State Data Commons.

Site	10Hz Data/full processed dataset	Ameriflux
US-INa	Richardson et al. (2023a) - https://doi.org/10.26208/CJTC-KS26 Horne et al. (2025b) - https://doi.org/10.26208/BV87-RP98	Davis (2023a) - https://doi.org/10.17190/AMF/2001300
US-INb	Richardson et al. (2023a) - https://doi.org/10.26208/CJTC-KS26 Horne et al. (2025b) - https://doi.org/10.26208/BV87-RP98	Davis (2023b) - https://doi.org/10.17190/AMF/2001301
US-INc	Richardson et al. (2023b) - https://doi.org/10.26208/fsy8-h855 Horne et al. (2025c) - https://doi.org/10.26208/E8CE-ZH47	Davis (2023c) - https://doi.org/10.17190/AMF/1987603
US-INd	Richardson et al. (2023c) - https://doi.org/10.26208/2NT2-RS82 Horne et al. (2025d) - https://doi.org/10.26208/900V-YJ22	Davis (2023d) - https://doi.org/10.17190/AMF/2001302
US-INe	Richardson et al. (2023c) - https://doi.org/10.26208/2NT2-RS82 Horne et al. (2025d) - https://doi.org/10.26208/900V-YJ22	Davis (2023e) - https://doi.org/10.17190/AMF/2001303
US-INf	Sarmiento and Davis (2017) - https://doi.org/10.17190/AMF/2001304	Davis (2023f) - https://doi.org/10.17190/AMF/2001304
US-INg	Richardson et al. (2023b) - https://doi.org/10.26208/fsy8-h855 Horne et al. (2025c) - https://doi.org/10.26208/E8CE-ZH47	Davis (2023g) - https://doi.org/10.17190/AMF/2001305
US-INi	Richardson et al. (2023c) - https://doi.org/10.26208/2NT2-RS82 Horne et al. (2025d) - https://doi.org/10.26208/900V-YJ22	Davis (2023h) - https://doi.org/10.17190/AMF/2001306
US-INj	Richardson et al. (2023c) - https://doi.org/10.26208/2NT2-RS82	Davis (2023i) - https://doi.org/10.17190/AMF/2001307

US-INn	Horne et al. (2025d) - https://doi.org/10.26208/900V-YJ22 Richardson et al. (2023c) - https://doi.org/10.26208/2NT2-RS82 Horne et al. (2025d) - https://doi.org/10.26208/900V-YJ22	Davis (2023j) - https://doi.org/10.17190/AMF/2001308
US-INp	Richardson et al. (2023c) - https://doi.org/10.26208/2NT2-RS82 Horne et al. (2025d) - https://doi.org/10.26208/900V-YJ22	Davis (2023k) - https://doi.org/10.17190/AMF/2001309

In addition, all INFLUX EC datasets are available through the Ameriflux network (https://ameriflux.lbl.gov/, Table 5). As of May 2025, the operation of all INFLUX flux towers has concluded. Data collected in 2025 at US-INg and US-INc sites will be processed, updated, and made available through all datasets in Table 5.

These flux measurements were a component of a broader research effort, the Indianapolis Flux Experiment (INFLUX). Multiple additional measurements and model data sets exist, creating a more complete experimental data set to assess urban greenhouse gases in Indianapolis, IN. These include mole fraction measurements (Miles et al., 2017b), flask measurements (https://gml.noaa.gov/dv/site/?stacode=INX), Doppler lidar measurements (https://csl.noaa.gov/projects/influx/), anthropogenic emissions inventories (Gurney et al., 2018), aircraft measurements (https://influx.psu.edu/influx/data/flight/), Vegetation Photosynthesis and Respiration Model (VPRM) simulations (Horne and Davis, 2024; Murphy et al., 2024), and Weather Research and Forecast (WRF) Reanalysis (Deng et al., 2020), which are not described in detail here. For more information concerning the INFLUX Project and the data collected, please visit https://influx.psu.edu. Most of these complementary data sets can be found at Penn State's Data Commons.

4 Conclusions

The INFLUX EC network has become a vital component of the multivariate INFLUX data set. Micrometeorological methods like EC can bridge the gap between land surface modeling and atmospheric inverse methods used to quantify urban GHG fluxes. The INFLUX EC flux data expands the growing database of urban flux measurements. Data representative of the range of land-atmosphere fluxes encountered in this region was obtained by deploying multiple sites representative of the land cover of the city and its surroundings. We hope the data availability will support cross-collaboration between projects involving urban environments.

Author contributions. NM, SR, and KD conceived and coordinated the INFLUX project. KD conceptualized the EC flux measurement strategies for INFLUX. SR and NM installed the instrumentation, and SR, NM, and BA worked on maintaining the currently deployed instruments. BJH oversaw the development and implementation of the data acquisition and monitoring system, and BJH and JH collaborated to create it. BA, HK, SM, and JH oversee data processing and quality control. JH led

the writing of this document, and all authors contributed to its editing and review. SM and JH helped create footprint climatologies for heterogeneous urban towers.

Competing interests. The authors declare that they have no conflict of interest.

Acknowledgements.
We thank Brady Hardiman for assistance in locating the sites for US-INa and US-INb, and the Crown Hill Cemetery and The Fort Golf Resort for access to these sites. We thank Hal Truax, Dave Rhoads, and Andy Mohr for allowing us to deploy flux towers on their property. We thank Daniel Sarmiento for leading the instrumentation and data acquisition from US-INf's EC flux measurements.

Financial support.

This work was supported by the US National Institute of Standards and Technology's urban GHG testbeds program, award numbers 70NANB10H245, 70NANB23H188, 70NANB19H128, and 70NANB15H336. HK was partly supported by Penn State's Institute of Energy and the Environment.

References

Aubinet, M., Vesala Timo, and Papale, D.: Eddy Covariance, edited by: Aubinet, M., Vesala, T., and Papale, D., Springer Netherlands, Dordrecht, 0–438 pp., 2012.

Baldocchi, D., Falge, E., Gu, L., Olson, R., Hollinger, D., Running, S., Anthoni, P., Bernhofer, C., Davis, K., Evans, R., Fuentes, J., Goldstein, A., Katul, G., Law, B., Lee, X., Malhi, Y., Meyers, T., Munger, W., Oechel, W., Paw, K. T., Pilegaard, K., Schmid, H. P., Valentini, R., Verma, S., Vesala, T., Wilson, K., and Wofsy, S.: FLUXNET: A New Tool to Study the Temporal and Spatial Variability of Ecosystem–Scale Carbon Dioxide, Water Vapor, and Energy Flux Densities, Bull Am Meteorol Soc, 82, 2415–2434, https://doi.org/10.1175/1520-0477(2001)082<2415:FANTTS>2.3.CO;2, 2001.

Barr, A.G., Richardson, A.D., Hollinger, D.Y., Papale, D., Arain, M.A., Black T.A., Bohrer, G., Dragoni, D., Fischer, M.L., Gu, L., Law, B.E., Margolis, H.A., McCaughey J.H., Munger J.W., Oechel, W., Schaeffer, K.: Use of change-point detection for friction–velocity threshold evaluation in eddy-covariance studies, Agricultural and Forest Meteorology, 171–172, 31-45, https://doi.org/10.1016/j.agrformet.2012.11.023, 2013.

Biraud, S., Chen, J., Christen, A., Davis, K., Lin, J., McFadden, J., Miller, C., Nemitz, E., Schade, G., Stagakis, S., Turnbull, J., and Vogt, T.: Eddy Covariance Measurements in Urban Environments: White paper prepared by the AmeriFlux Urban Fluxes ad hoc committee, 2021.

Bou-Zeid, E., Anderson, W., Katul, G. G., and Mahrt, L.: The Persistent Challenge of Surface Heterogeneity in Boundary-Layer Meteorology: A Review, Boundary Layer Meteorol, 177, 227–245, https://doi.org/10.1007/s10546-020-00551-8, 2020.

Burba, G.: Eddy Covariance Method for Scientific, Industrial, Agricultural, and Regulatory Applications; a field book on measuring ecosystem gas exchange and areal emission rates, LI-COR Biosciences, Lincoln, Nebraska, xii–331 pp., 2013.

Butterworth, B.J., Desai, A.R., Metzger, S., Townsend, P.A., Schwartz, M.D., Petty, G.W., Mauder, M., Vogelmann, H., Andresen, C.G., Augustine, T.J., Bertram, T.H., Brown, W.O.J., Buban, M., Cleary, P., Durden, D.J., Florian, C.R., Ruiz, E.G., Iglinski, T.J., Kruger, E.L., Lantz, K., Lee, T.R., Meyers, T.P., Mineau, J.K., Olson, E.R., Oncley, S.P., Paleri, S., Pertzborn, R.A., Pettersen, C., Plummer , D.M., Riihimaki, L., Sedlar, J., Smith, E.N., Speidel, J., Stoy, P.C., Sühring, M., Thom, J.E., Turner, D.D., Vermeuel, M.P., Wagner, T.J., Wang, Z., Wanner, L., White, L.D., Wilczak, J.M.M., Wright, D.B., and Zheng, T.: Connecting Land-Atmosphere Interactions to Surface Heterogeneity in CHEESEHEAD19, Bulletin of the American Meteorological Society, 102(2), E421-E445, doi:10.1175/BAMS-D-19-0346.1, 2021.

Chu, H., Luo, X., Ouyang, Z., Chan, W. S., Dengel, S., Biraud, S. C., Torn, M. S., Metzger, S., Kumar, J., Arain, M. A., Arkebauer, T. J., Baldocchi, D., Bernacchi, C., Billesbach, D., Black, T. A., Blanken, P. D., Bohrer, G., Bracho, R., Brown, S., Brunsell, N. A., Chen, J., Chen, X., Clark, K., Desai, A. R., Duman, T., Durden, D., Fares, S., Forbrich, I., Gamon, J. A., Gough, C. M., Griffis, T., Helbig, M., Hollinger, D., Humphreys, E., Ikawa, H., Iwata, H., Ju, Y., Knowles, J. F., Knox, S. H., Kobayashi, H., Kolb, T., Law, B., Lee, X., Litvak, M., Liu, H., Munger, J. W., Noormets, A., Novick, K., Oberbauer, S. F., Oechel, W., Oikawa, P., Papuga, S. A., Pendall, E., Prajapati, P., Prueger, J., Quinton, W. L., Richardson, A. D., Russell, E. S., Scott, R. L., Starr, G., Staebler, R., Stoy, P. C., Stuart-Haëntjens, E., Sonnentag, O., Sullivan, R. C., Suyker, A., Ueyama, M., Vargas, R., Wood, J. D., and Zona, D.: Representativeness of Eddy-Covariance flux footprints for areas surrounding AmeriFlux sites, Agric For Meteorol, 301–302, https://doi.org/10.1016/j.agrformet.2021.108350, 2021.

Crawford, B. and Christen, A.: Spatial source attribution of measured urban eddy covariance CO2 fluxes, Theor Appl Climatol, 119, 733–755, https://doi.org/10.1007/s00704-014-1124-0, 2015.

Davis, K. J., Deng, A., Lauvaux, T., Miles, N. L., Richardson, S. J., Sarmiento, D. P., Gurney, K. R., Hardesty, R. M., Bonin, T. A., Brewer, W. A., Lamb, B. K., Shepson, P. B., Harvey, R. M., Cambaliza, M. O., Sweeney, C., Turnbull, J. C., Whetstone, J., and Karion, A.: The Indianapolis Flux Experiment (INFLUX): A test-bed for developing urban greenhouse gas emission measurements, Elementa: Science of the Anthropocene, 5, https://doi.org/10.1525/elementa.188, 2017.

Davis, K.J., P.S. Bakwin, B.W. Berger, C. Yi, C. Zhao, R.M. Teclaw and J.G. Isebrands.: The annual cycle of CO_2 and H_2O exchange over a northern mixed forest as observed from a very tall tower. Global Change Biology, 9, 1278-1293, 2003.

Davis K. J. AmeriFlux BASE US-INa INFLUX - Cemetery Turfgrass Tower, Ver. 1-5, AmeriFlux AMP, (data set), https://doi.org/10.17190/AMF/2001300, 2023a.

Davis K. J. AmeriFlux BASE US-INb INFLUX - Golf Course, Ver. 1-5, AmeriFlux AMP, (data set), https://doi.org/10.17190/AMF/2001301, 2023b.

Davis K. J. AmeriFlux BASE US-INc INFLUX - Downtown Indianapolis (Site-3), Ver. 1-5, AmeriFlux AMP, (data set), https://doi.org/10.17190/AMF/1987603, 2023c.

Davis K. J. AmeriFlux BASE US-INd INFLUX - Agricultural Site East near Pittsboro, Ver. 1-5, AmeriFlux AMP, (data set), https://doi.org/10.17190/AMF/2001302, 2023d.

Davis K. J. AmeriFlux BASE US-INe INFLUX - Agricultural Site West near Pittsboro, Ver. 1-5, AmeriFlux AMP, (data set), https://doi.org/10.17190/AMF/2001303, 2023e.

Davis K. J. AmeriFlux BASE US-INf INFLUX - East 21st St (Site 2), Ver. 1-5, AmeriFlux AMP, (data set), https://doi.org/10.17190/AMF/2001304, 2023f.

Davis K. J. AmeriFlux BASE US-INg INFLUX - Wayne Twp Comm (Site-7), Ver. 1-5, AmeriFlux AMP, (data set), https://doi.org/10.17190/AMF/2001305, 2023g.

Davis K. J. AmeriFlux BASE US-INi INFLUX - Agricultural Site East of Indianapolis (Site-9a), Ver. 1-5, AmeriFlux AMP, (data set), https://doi.org/10.17190/AMF/2001306, 2023h.

Davis K. J. AmeriFlux BASE US-INj INFLUX - Agricultural Site East of Indianapolis (Site-9b), Ver. 1-5, AmeriFlux AMP, (data set), https://doi.org/10.17190/AMF/2001307, 2023i.

Davis K. J. AmeriFlux BASE US-INn INFLUX - Agricultural Site West of Indianapolis (Site-14a), Ver. 1-5, AmeriFlux AMP, (data set), https://doi.org/10.17190/AMF/2001308, 2023j.

Davis K. J. AmeriFlux BASE US-INn INFLUX - Agricultural Site West of Indianapolis (Site-14b), Ver. 1-5, AmeriFlux AMP, (data set), https://doi.org/10.17190/AMF/2001309, 2023k.

Davis, K., Zaitchik, B., Asa-Awuku, A., Bou-Zeid, E., Baidar, S., Boxe, C., Brewer, W. A., Chiao, S., Damoah, R., Decarlo, P., Demoz, B., Dickerson, R., Giometto, M., Gonzalez-Cruz, J., Jensen, M., Kuang, C., Lamer, K., Li, X., Lombardo, K., Miles, N., Niyogi, D., Pan, Y., Peters, J., Ramamurthy, P., Peng, W., Richardson, S., Sakai, R., Waugh, D., and Zhang, J.: Coastal-Urban-Rural Atmospheric Gradient Experiment (CoURAGE) Science Plan, 1–50 pp., 2024.

Dennis, L.; Richardson, S.; Miles, N.; Woda, J.; Brantley, S.; Davis, K.: Measurements of Atmospheric Methane Emissions from Stray Gas Migration: A Case Study from the Marcellus Shale. ACS Earth Space Chem, 6, 4, 909–919, https://doi.org/10.1021/acsearthspacechem.1c00312, 2022.

Desjardins, R.L., P.H. Schuepp, J.I. MacPherson, and D.J. Buckley.: Spatial and temporal variations of the fluxes of carbon dioxide and sensible and latent heat over the FIFE site. *J.* Geophys. Res. 97: 18 467–18 475, 1992.

Deng, A., Lauvaux, T., Miles, N. L., Davis, K. J., Barkley, Z. R. Meteorological fields over Indianapolis, IN from the Weather Research and Forecasting model (WRF v3.5.1), Penn State DataCommons [data set], https://doi.org/10.26208/z04g-3h91, 2020.

De Ridder, K.: Bulk Transfer Relations for the Roughness Sublayer, Boundary Layer Meteorology, 134, 257–267, https://doi.org/10.1007/s10546-009-9450-y, 2010.

Dragoni, D., Schmid, H. P., Wayson, C., Potters, H., Grimmond, S., and Randolph, J.: Evidence of increased net ecosystem productivity associated with a longer vegetated season in a deciduous forest in south-central Indiana, USA, Glob Chang Biol, 17, 886–897, https://doi.org/10.1111/j.1365-2486.2010.02281.x, 2011.

Dyer, A. J.: A review of flux-profile relationships, Boundary Layer Meteorology, 7, 363–372, https://doi.org/10.1007/BF00240838, 1974.

Eder, F., Schmidt, M., Damian, T., Träumner, K., and Mauder, M.: Mesoscale Eddies Affect Near-Surface Turbulent Exchange: Evidence from Lidar and Tower Measurements, J Appl Meteorol Climatol, 54, 189–206, https://doi.org/10.1175/JAMC-D-14-0140.1, 2015a.

Eder, F., De Roo, F., Rotenberg, E., Yakir, D., Schmid, H. P., and Mauder, M.: Secondary circulations at a solitary forest surrounded by semi-arid shrubland and their impact on eddy-covariance measurements, Agric For Meteorol, 211–212, 115–127, https://doi.org/10.1016/j.agrformet.2015.06.001, 2015b.

Feigenwinter, C., Vogt, R., and Christen, A.: Eddy Covariance Measurements Over Urban Areas, in: Eddy Covariance, Springer Netherlands, Dordrecht, 377–397, https://doi.org/10.1007/978-94-007-2351-1_16, 2012.

Foken, T.: Micrometeorology, Carmen J. Nappo., Springer, 2008.

Foken, Th. and Wichura, B.: Tools for quality assessment of surface-based flux measurements, Agric For Meteorol, 78, 83–105, https://doi.org/10.1016/0168-1923(95)02248-1, 1996.

Gurney KR, Razlivanov I, Song Y, Zhou Y, Benes B, Abdul-Massih M.: Quantification of Fossil Fuel CO $_2$ Emissions on the Building/Street Scale for a Large U.S. City. Environ Sci Technol 46(21): 12194–12202. doi: 10.1021/es3011282, 2012.

Gurney, K. R., Patarasuk R., Liang, J., Yuyu, Z., O'Keeffe, D., Hutchins, M., Huang, J., Song, Y., Rao, P., Wong, T. M., Whetstone, J. R., Hestia Fossil Fuel Carbon Dioxide Emissions for Indianapolis, Indiana, National Institute of Standards and Technology, NIST Public Data Repository [data set], https://doi.org/10.18434/T4/1503341, 2018.

Hersbach, H., Bell, B., Berrisford, P., Biavati, G., Horányi, A., Muñoz Sabater, J., Nicolas, J., Peubey, C., Radu, R., Rozum, I., Schepers, D., Simmons, A., Soci, C., Dee, D., Thépaut, J-N., ERA5 hourly data on single levels from 1940 to present. Copernicus Climate Change Service (C3S) Climate Data Store (CDS) [data set], https://doi.org/10.24381/cds.adbb2d47, 2023.

Horne, J. P., Davis, K. J. Vegetation Photosynthesis and Respiration Model (VPRM) run for 2019 over Indianapolis, IN, using a turfgrass PFT, Penn State DataCommons [data set], https://doi.org/10.26208/zs32-5n02, 2024.

Horne, J. P., Jin, C., Miles, N. L., Richardson, S. J., Murphy, S. L., Wu, K., and Davis, K. J.: The Impact of Turfgrass on Urban Carbon Dioxide Fluxes in Indianapolis, Indiana, USA, https://doi.org/10.1029/2024JG008477, 2025a.

Horne, J., K. J. Davis, S. J. Richardson, N. L. Miles, S. Murphy, B. J. Haupt, H. Kenion, and B. Ahlswede. Turfgrass INFLUX Eddy Covariance Towers - Processed 30-Minute Data. Penn State Data Commons [data set], https://doi.org/10.26208/BV87-RP98, 2025b.

673 Horne, J., K. J. Davis, S. J. Richardson, N. L. Miles, S. Murphy, B. J. Haupt, H. Kenion, and B.
674 Ahlswede. Mixed Urban INFLUX Eddy Covariance Towers - Processed 30-Minute Data. Penn State Data
675 Commons [data set], https://doi.org/10.26208/BV87-RP98, 2025c.

676 Horne, J., K. J. Davis, S. J. Richardson, N. L. Miles, S. Murphy, B. J. Haupt, H. Kenion, and B.
677 Ahlswede. Agricultural INFLUX Eddy Covariance Towers - Processed 30-Minute Data. Penn State Data
678 Commons [data set], https://doi.org/10.26208/900V-YJ22, 2025d.

679 Horst, T.W., and J.C. Weil.: Footprint estimation for scalar flux measurements in the atmospheric surface
680 layer. Boundary Layer Meteorol. **59**: 279–296, 1992.

681 Järvi, L., Rannik, U., Kokkonen, T. V., Kurppa, M., Karppinen, A., Kouznetsov, R. D., Rantala, P., Vesala,
682 T., and Wood, C. R.: Uncertainty of eddy covariance flux measurements over an urban area based on two
683 towers, Atmos Meas Tech, 11, 5421–5438, https://doi.org/10.5194/amt-11-5421-2018, 2018.

684 Kaimal, J. C., Wyngaard, J. C., Izumi, Y., and Coté, O. R.: Spectral characteristics of surface-layer
685 turbulence, Quarterly Journal of the Royal Meteorological Society, 98, 563–589,
686 https://doi.org/10.1002/qj.49709841707, 1972.

687 Kang, S., K.J. Davis and M.A. LeMone.: Observations of the ABL structures over a heterogeneous land
688 surface during IHOP_2002. J. Hydrometeorology, 8, 221-244, DOI: 10.1175/JHM567.1, 2007.

689 Karion, A., Ghosh, S., Lopez-Coto, I., Mueller, K., Gourdji, S., Pitt, J., and Whetstone, J.: Methane
690 Emissions Show Recent Decline but Strong Seasonality in Two US Northeastern Cities, Environ Sci
691 Technol, 57, 19565–19574, https://doi.org/10.1021/acs.est.3c05050, 2023.

692 Kenion, H. C., Davis, K. J., Miles, N. L., Monteiro, V. C., Richardson, S. J., and Horne, J. P.: Estimation
693 of Urban Greenhouse Gas Fluxes from Mole Fraction Measurements Using Monin–Obukhov Similarity
694 Theory, J Atmos Ocean Technol, 41, 833–846, https://doi.org/10.1175/JTECH-D-23-0164.1, 2024.

695 Kent, C. W., Lee, K., Ward, H. C., Hong, J. W., Hong, J., Gatey, D., and Grimmond, S.: Aerodynamic
696 roughness variation with vegetation: analysis in a suburban neighbourhood and a city park, Urban
697 Ecosyst, 21, 227–243, https://doi.org/10.1007/s11252-017-0710-1, 2018.

698 Kljun, N., Calanca, P., Rotach, M. W., and Schmid, H. P.: A simple two-dimensional parameterisation for
699 Flux Footprint Prediction (FFP), Geosci Model Dev, 8, 3695–3713, https://doi.org/10.5194/gmd-8-3695-
700 2015, 2015.

701 Kotthaus, S. and Grimmond, C. S. B.: Energy exchange in a dense urban environment – Part I: Temporal
702 variability of long-term observations in central London, Urban Clim, 10, 261–280,
703 https://doi.org/10.1016/j.uclim.2013.10.002, 2014.

704 Lan, C., Mauder, M., Stagakis, S., Loubet, B., D'Onofrio, C., Metzger, S., Durden, D., and Herig-
705 Coimbra, P.-H.: Intercomparison of eddy-covariance software for urban tall-tower sites, Atmos Meas
706 Tech, 17, 2649–2669, https://doi.org/10.5194/amt-17-2649-2024, 2024.

Lauvaux, T., Gurney, K. R., Miles, N. L., Davis, K. J., Richardson, S. J., Deng, A., Nathan, B. J., Oda, T., Wang, J. A., Hutyra, L., and Turnbull, J.: Policy-relevant assessment of urban CO2 emissions, Environ Sci Technol, 54, 10237–10245, https://doi.org/10.1021/acs.est.0c00343, 2020.

Lee, X. and Massman, W. J.: A Perspective on Thirty Years of the Webb, Pearman and Leuning Density Corrections, Boundary Layer Meteorol, 139, 37–59, https://doi.org/10.1007/s10546-010-9575-z, 2011.

Lee, X., Massman, W., and Law, B.: Handbook of Micrometeorology, edited by: Lee, X., Massman, W., and Law, B., Springer Netherlands, Dordrecht, 1–250 pp., https://doi.org/10.1007/1-4020-2265-4, 2004.

Lipson, M., Grimmond, S., Best, M., Chow, W. T. L., Christen, A., Chrysoulakis, N., Coutts, A., Crawford, B., Earl, S., Evans, J., Fortuniak, K., Heusinkveld, B. G., Hong, J.-W., Hong, J., Järvi, L., Jo, S., Kim, Y.-H., Kotthaus, S., Lee, K., Masson, V., McFadden, J. P., Michels, O., Pawlak, W., Roth, M., Sugawara, H., Tapper, N., Velasco, E., and Ward, H. C.: Harmonized gap-filled datasets from 20 urban flux tower sites, Earth Syst Sci Data, 14, 5157–5178, https://doi.org/10.5194/essd-14-5157-2022, 2022.

Liu, H. Z., Feng, J. W., Järvi, L., and Vesala, T.: Four-year (2006-2009) eddy covariance measurements of CO 2 flux over an urban area in Beijing, Atmos Chem Phys, 12, 7881–7892, https://doi.org/10.5194/acp-12-7881-2012, 2012.

Lwasa, S., K.C. Seto, X. Bai, H. Blanco, K.R. Gurney, Ş. Kılkış, O. Lucon, J. Murakami, J. Pan, A. Sharifi, and Y. Yamagata: Urban Systems and Other Settlements, in: Climate Change 2022 - Mitigation of Climate Change, Cambridge University Press, 861–952, https://doi.org/10.1017/9781009157926.010, 2023.

Mauder, M. and Foken, T.: Documentation and Instruction Manual of the Eddy Covariance Software Package TK2, 1 pp., 2004.

Mauder, M., Foken, T., and Cuxart, J.: Surface-Energy-Balance Closure over Land: A Review, Boundary Layer Meteorol, 177, 395–426, https://doi.org/10.1007/s10546-020-00529-6, 2020.

Menzer, O. and McFadden, J. P.: Statistical partitioning of a three-year time series of direct urban net CO2 flux measurements into biogenic and anthropogenic components, Atmos Environ, 170, 319–333, https://doi.org/10.1016/j.atmosenv.2017.09.049, 2017.

Miles, N. L., Richardson, S. J., Lauvaux, T., Davis, K. J., Balashov, N. V., Deng, A., Turnbull, J. C., Sweeney, C., Gurney, K. R., Patarasuk, R., Razlivanov, I., Cambaliza, M. O. L., and Shepson, P. B.: Quantification of urban atmospheric boundary layer greenhouse gas dry mole fraction enhancements in the dormant season: Results from the Indianapolis Flux Experiment (INFLUX), Elementa: Science of the Anthropocene, 5, https://doi.org/10.1525/elementa.127, 2017a.

Miles, N. L., Richardson, S. J., Davis, K. J., Haupt, B. J.: In-situ tower atmospheric measurements of carbon dioxide, methane and carbon monoxide mole fraction for the Indianapolis Flux (INFLUX) project, Indianapolis, IN, USA., Penn State DataCommons [data set], https://doi.org/10.18113/D37G6P, 2017b.

741 Milesi, C., Running, S. W., Elvidge, C. D., Dietz, J. B., Tuttle, B. T., and Nemani, R. R.: Mapping and
742 Modeling the Biogeochemical Cycling of Turf Grasses in the United States, Environ Manage, 36, 426–
743 438, https://doi.org/10.1007/s00267-004-0316-2, 2005.

744 Miller, J. B., Lehman, S. J., Verhulst, K. R., Miller, C. E., Duren, R. M., Yadav, V., Newman, S., and
745 Sloop, C. D.: Large and seasonally varying biospheric CO 2 fluxes in the Los Angeles megacity revealed
746 by atmospheric radiocarbon, Proceedings of the National Academy of Sciences, 117, 26681–26687,
747 https://doi.org/10.1073/pnas.2005253117, 2020.

748 Moncrieff, J. B., Massheder, J. M., de Bruin, H., Elbers, J., Friborg, T., Heusinkveld, B., Kabat, P., Scott,
749 S., Soegaard, H., and Verhoef, A.: A system to measure surface fluxes of momentum, sensible heat, water
750 vapour and carbon dioxide, J Hydrol (Amst), 188–189, 589–611, https://doi.org/10.1016/S0022-
751 1694(96)03194-0, 1997.

752 Moore, C. J.: Frequency response corrections for eddy correlation systems, Boundary Layer Meteorol, 37,
753 17–35, https://doi.org/10.1007/BF00122754, 1986.

754 Murphy, S. L., Davis, K. J., Miles, N. L. Penn State Department of Meteorology Vegetation
755 Photosynthesis and Respiration Model (VPRM) runs for Indianapolis, IN, from 2012 through 2021, Penn
756 State DataCommons [data set], https://doi.org/10.26208/zs32-5n02, 2024.

757 Murphy, S. L., Davis, K. J., Miles, N. L., Barkley, Z. R., Deng, A., Horne, J. P., Richardson, S. J., and
758 Gourdji, S. M.: Simulating complex CO_2 background conditions for Indianapolis, IN, with a simple
759 ecosystem CO_2 flux model. Journal of Geophysical Research: Biogeosciences, 130, e2024JG008518.
760 https://doi.org/10.1029/2024JG008518, 2025.

761 Ng, B. J. L., Hutyra, L. R., Nguyen, H., Cobb, A. R., Kai, F. M., Harvey, C., and Gandois, L.: Carbon
762 fluxes from an urban tropical grassland, Environmental Pollution, 203, 227–234,
763 https://doi.org/10.1016/j.envpol.2014.06.009, 2015.

764 Nicolini, G., Antoniella, G., Carotenuto, F., Christen, A., Ciais, P., Feigenwinter, C., Gioli, B., Stagakis,
765 S., Velasco, E., Vogt, R., Ward, H. C., Barlow, J., Chrysoulakis, N., Duce, P., Graus, M., Helfter, C.,
766 Heusinkveld, B., Järvi, L., Karl, T., Marras, S., Masson, V., Matthews, B., Meier, F., Nemitz, E.,
767 Sabbatini, S., Scherer, D., Schume, H., Sirca, C., Steeneveld, G.-J., Vagnoli, C., Wang, Y., Zaldei, A.,
768 Zheng, B., and Papale, D.: Direct observations of CO2 emission reductions due to COVID-19 lockdown
769 across European urban districts, Science of The Total Environment, 830, 154662,
770 https://doi.org/10.1016/j.scitotenv.2022.154662, 2022.

771 Mahrt, L., D. Vickers, J. Sun.: Spatial variations of surface moisture flux from aircraft data, Advances in
772 Water Resources, 24, 9–10, 1133-1141, https://doi.org/10.1016/S0309-1708(01)00045-8. 2001.

773 Oncley, S. P., Lenschow, D. H., Campos, T. L., Davis, K. J., and Mann, J.: Regional-scale surface flux
774 observations across the boreal forest during BOREAS, Journal of Geophysical Research: Atmospheres,
775 102, 29147–29154, https://doi.org/10.1029/97JD00242, 1997.

776 Pahari, R., Leclerc, M. Y., Zhang, G., Nahrawi, H., and Raymer, P.: Carbon dynamics of a warm season
777 turfgrass using the eddy-covariance technique, Agric Ecosyst Environ, 251, 11–25,
778 https://doi.org/10.1016/j.agee.2017.09.015, 2018.

779 Papale, D., Antoniella, G., Nicolini, G., Gioli, B., Zaldei, A., Vogt, R., Feigenwinter, C., Stagakis, S.,
780 Chrysoulakis, N., Järvi, L., Nemitz, E., Helfter, C., Barlow, J., Meier, F., Velasco, E., Christen, A., and
781 Masson, V.: Clear evidence of reduction in urban CO 2 emissions as a result of COVID-19 lockdown
782 across Europe, 2020.

783 Papale, D., Andreas, C., Davis, K., Christian, F., Beniamino Gioli, Leena, J., Bradley, M., Erik, V., and
784 Roland, V.: Eddy covariance flux observations., GAW Report, 275, 114–123, 2022.

785 Pastorello, G., Trotta, C., Canfora, E., Chu, H., Christianson, D., Cheah, Y. W., Poindexter, C., Chen, J.,
786 Elbashandy, A., Humphrey, M., Isaac, P., Polidori, D., Ribeca, A., van Ingen, C., Zhang, L., Amiro, B.,
787 Ammann, C., Arain, M. A., Ardö, J., Arkebauer, T., Arndt, S. K., Arriga, N., Aubinet, M., Aurela, M.,
788 Baldocchi, D., Barr, A., Beamesderfer, E., Marchesini, L. B., Bergeron, O., Beringer, J., Bernhofer, C.,
789 Berveiller, D., Billesbach, D., Black, T. A., Blanken, P. D., Bohrer, G., Boike, J., Bolstad, P. V., Bonal, D.,
790 Bonnefond, J. M., Bowling, D. R., Bracho, R., Brodeur, J., Brümmer, C., Buchmann, N., Burban, B.,
791 Burns, S. P., Buysse, P., Cale, P., Cavagna, M., Cellier, P., Chen, S., Chini, I., Christensen, T. R., Cleverly,
792 J., Collalti, A., Consalvo, C., Cook, B. D., Cook, D., Coursolle, C., Cremonese, E., Curtis, P. S.,
793 D'Andrea, E., da Rocha, H., Dai, X., Davis, K. J., De Cinti, B., de Grandcourt, A., De Ligne, A., De
794 Oliveira, R. C., Delpierre, N., Desai, A. R., Di Bella, C. M., di Tommasi, P., Dolman, H., Domingo, F.,
795 Dong, G., Dore, S., Duce, P., Dufrêne, E., Dunn, A., Dušek, J., Eamus, D., Eichelmann, U., ElKhidir, H.
796 A. M., Eugster, W., Ewenz, C. M., Ewers, B., Famulari, D., Fares, S., Feigenwinter, I., Feitz, A., Fensholt,
797 R., Filippa, G., Fischer, M., Frank, J., Galvagno, M., Gharun, M., Gianelle, D., et al.: The
798 FLUXNET2015 dataset and the ONEFlux processing pipeline for eddy covariance data, Sci Data, 7, 225,
799 https://doi.org/10.1038/s41597-020-0534-3, 2020.

800 Paw U, K. T., Baldocchi, D. D., Meyers, T. P., and Wilson, K. B.: Correction Of Eddy-Covariance
801 Measurements Incorporating Both Advective Effects And Density Fluxes, Boundary Layer Meteorol, 97,
802 487–511, https://doi.org/10.1023/A:1002786702909, 2000.

803 Pawlak, W. and Fortuniak, K.: Eddy covariance measurements of the net turbulent methane flux in the
804 city centre-results of 2-year campaign in Lodz, Poland, Atmos Chem Phys, 16, 8281–8294,
805 https://doi.org/10.5194/acp-16-8281-2016, 2016.

806 Pérez-Ruiz, E. R., Vivoni, E. R., and Templeton, N. P.: Urban land cover type determines the sensitivity
807 of carbon dioxide fluxes to precipitation in Phoenix, Arizona, PLoS One, 15,
808 https://doi.org/10.1371/journal.pone.0228537, 2020.

809 Peters, E. B. and McFadden, J. P.: Continuous measurements of net CO2 exchange by vegetation and
810 soils in a suburban landscape, J Geophys Res Biogeosci, 117, https://doi.org/10.1029/2011JG001933,
811 2012.

812 Peters, E. B., Hiller, R. V., and McFadden, J. P.: Seasonal contributions of vegetation types to suburban
813 evapotranspiration, J Geophys Res Biogeosci, 116, https://doi.org/10.1029/2010JG001463, 2011.

Raut, B. A., Muradyan, P., Pal, S., Ivans, S., Tuftedal, M., Sherman, Z., Grover, M., O'Brien, J., Jackson, R., Wawrzyniak, E., Cho, A., Anderson, G., Gala, T., and Collis, S.: The Chicago Urban Flux Network with Perspectives from an Eddy Covariance Workshop, Bull Am Meteorol Soc, 106, E1724–E1730, https://doi.org/10.1175/BAMS-D-25-0180.1, 2025.

Richardson, S. J., Miles, N. L., Davis, K. J., Lauvaux, T., Martins, D. K., Turnbull, J. C., McKain, K., Sweeney, C., and Cambaliza, M. O. L.: Tower measurement network of in-situ CO2, CH4, and CO in support of the Indianapolis FLUX (INFLUX) Experiment, Elementa: Science of the Anthropocene, 5, https://doi.org/10.1525/elementa.140, 2017.

Richardson, S. J., Miles, N. L., Haupt, B. J., Ahlswede, B., Horne, J. P., Davis, K. J. Eddy Covariance High-Frequency Data for Turfgrass and Pasture in Indianapolis, Indiana and Montgomery County, Maryland (US-INa, US-INb, US-BWa, US-BWb, US-BWc), Penn State DataCommons [data set], https://doi.org/10.26208/CJTC-KS26, 2023a.

Richardson, S. J., Miles, N. L., Haupt, B. J., Ahlswede, B., Horne, J. P., Davis, K. J. Eddy Covariance High-Frequency Data for Agricultural Sites near Indianapolis, Indiana (US-INd, US-INe, US-INi, US-INj, US-INn, US-INp), Penn State DataCommons [data set], https://doi.org/10.26208/fsy8-h855, 2023b.

Richardson, S. J., Miles, N. L., Haupt, B. J., Ahlswede, B., Horne, J. P., Davis, K. J. Eddy Covariance High-Frequency Data for Urban and Suburban Sites in Indianapolis, Indiana (US-INc, US-INg), Penn State DataCommons [data set], https://doi.org/10.26208/2NT2-RS82, 2023c.

Sarmiento, D. P., Davis, K. J., Deng, A., Lauvaux, T., Brewer, A., and Hardesty, M.: A comprehensive assessment of land surface-atmosphere interactions in a WRF/Urban modeling system for Indianapolis, IN, Elementa: Science of the Anthropocene, 5, https://doi.org/10.1525/elementa.132, 2017.

Sarmiento, D. P., Davis, K. J. Eddy covariance flux tower data for Indianapolis, IN (INFLUX project), Penn State DataCommons [data set], https://doi.org/10.17190/AMF/2001304, 2017.

Schmid, H. P., Grimmond, S., Cropley, F., Offerle, B., and Su, H.-B.: Measurements of CO2 and energy fluxes over a mixed hardwood forest in the mid-western United States, Agric For Meteorol, 103, 357–374, https://doi.org/10.1016/S0168-1923(00)00140-4, 2000.

Schuepp, P. H., Leclerc, M. Y., MacPherson, J. I., and Desjardins, R. L.: Footprint prediction of scalar fluxes from analytical solutions of the diffusion equation, Boundary Layer Meteorol, 50, 355–373, https://doi.org/10.1007/BF00120530, 1990.

Semerjian, H. G. and Whetstone, J. R.: Urban greenhouse gas measurements :, https://doi.org/10.6028/NIST.TN.2145, 2021.

Shi, Y., K. J. Davis, C. J. Duffy, X. Yu.: Development of a Coupled Land Surface Hydrologic Model and Evaluation at a Critical Zone Observatory. J. Hydrometeor, 14, 1401–1420, 2013.

Stewart, I. D. and Oke, T. R.: Local climate zones for urban temperature studies, Bull Am Meteorol Soc, 93, 1879–1900, https://doi.org/10.1175/BAMS-D-11-00019.1, 2012.

Sun, L., Chen, J., Li, Q., and Huang, D.: Dramatic uneven urbanization of large cities throughout the world in recent decades, Nat Commun, 11, 5366, https://doi.org/10.1038/s41467-020-19158-1, 2020.

Southwest Integrated Field Laboratory (SW-IFL): 2024 Annual Report – Addressing extreme heat and associated environmental and societal stressors through resilient solutions & next-generation predictive tools, DOE Award #DE-SC0023520, U.S. Department of Energy, Washington, D.C., USA, 2024

Turnbull, J. C., Karion, A., Davis, K. J., Lauvaux, T., Miles, N. L., Richardson, S. J., Sweeney, C., McKain, K., Lehman, S. J., Gurney, K. R., Patarasuk, R., Liang, J., Shepson, P. B., Heimburger, A., Harvey, R., and Whetstone, J.: Synthesis of Urban CO 2 Emission Estimates from Multiple Methods from the Indianapolis Flux Project (INFLUX), Environ Sci Technol, 53, 287–295, https://doi.org/10.1021/acs.est.8b05552, 2019.

Turnbull, J. C., Curras, T., Gurney, K. R., Hilton, T. W., Mueller, K. L., Vogel, F., Yao, B., Albarus, I., Ars, S., Baidar, S., Chatterjee, A., Chen, H., Chen, J., Christen, A., Davis, K. J., Hajny, K., Han, P., Karion, A., Kim, J., Lopez Coto, I., Papale, D., Ramonet, M., Sperlich, P., Vardag, S. N., Vermeulen, A., Vimont, I. J., Wu, D., Zhang, W., Augusti-Panareda, A., Ahlgren, K., Ahn, D., Boyle, T., Brewer, A., Brunner, D., Cai, Q., Chambers, S., Chen, Z., Dadheech, N., D'Onofrio, C., Dunse, B. L., Engelen, R., Fathi, S., Gioli, B., Hammer, S., Hase, F., Hong, J., Hutyra, L. R., Järvi, L., Jeong, S., Karstens, U., Kenion, H. C., Kljun, N., Laurent, O., Lauvaux, T., Lin, J. C., Liu, Z., Loh, Z., Maier, F., Matthews, B., Mauder, M., Miles, N., Mitchell, L., Monteiro, V. C., Mostafavi Pak, N., Röckmann, T., Roiger, A., Roten, D., Scheutz, C., Shahrokhi, N., Shepson, P. B., Stagakis, S., Tong, X., Trudinger, C. M., Velasco, E., Whetstone, J. R., Winbourne, J. B., Wu, J., Xueref-Remy, I., Yadav, V., Yu, L., Zazzeri, G., Zeng, N., and Zhou, M.: IG3IS Urban Greenhouse Gas Emission Observation and Monitoring Good Research Practice Guidelines, WMO GAW Report 275, World Meteorological Organisation, Geneva, Switzerland, 2025.

U.S. Department of Agriculture, Natural Resource Conservation Service (NRCS), Indiana State Office, and the Indiana Geographic Information Council (IGIC), under separate BAA Agreements in partnership with the United States Geological Services (USGS) 3DEP Program. Indiana 3DEP Lidar Base Products. (data set), https://igic.memberclicks.net/indiana-s-new-3dep-lidar-data-and-informational-resources, 2021.

Vickers, D. and Mahrt, L.: Quality Control and Flux Sampling Problems for Tower and Aircraft Data, J Atmos Ocean Technol, 14, 512–526, https://doi.org/10.1175/1520-0426(1997)014<0512:QCAFSP>2.0.CO;2, 1997.

Vogel, E., Davis, K. J., Wu, K., Miles, N. L., Richardson, S. J., Gurney, K. R., Monteiro, V., Roest, G. S., Kenion, H. C. R., and Horne, J. P.: Using eddy-covariance to measure the effects of COVID-19 restrictions on CO 2 emissions in a neighborhood of Indianapolis, IN, Carbon Manag, 15, https://doi.org/10.1080/17583004.2024.2365900, 2024.

Vogt, R., Christen, A., Rotach, M. W., Roth, M., and Satyanarayana, A. N. V.: Temporal dynamics of CO2 fluxes and profiles over a Central European city, Theor Appl Climatol, 84, 117–126, https://doi.org/10.1007/s00704-005-0149-9, 2006.

Wang, W., K. J. Davis, B. D. Cook, M. P. Butler, D. M. Ricciuto.: Decomposing CO_2 fluxes measured over a mixed ecosystem at a tall tower and extending to a region: A case study, Journal of Geophysical Research Biogeosciences, 111(G2), G02005, doi:10.1029/2005JG000093, 2006.

Ward, H. C., Rotach, M. W., Gohm, A., Graus, M., Karl, T., Haid, M., Umek, L., and Muschinski, T.: Energy and mass exchange at an urban site in mountainous terrain - the Alpine city of Innsbruck, Atmos Chem Phys, 22, 6559–6593, https://doi.org/10.5194/acp-22-6559-2022, 2022.

Webb, E. K., Pearman, G. I., and Leuning, R.: Correction of flux measurements for density effects due to heat and water vapour transfer, Quarterly Journal of the Royal Meteorological Society, 106, 85–100, https://doi.org/10.1002/qj.49710644707, 1980.

Wilczak, J. M., Oncley, S. P., and Stage, S. A.: Sonic Anemometer Tilt Correction Algorithms, Boundary Layer Meteorol, 99, 127–150, https://doi.org/10.1023/A:1018966204465, 2001.

Wu, K., Davis, K. J., Miles, N. L., Richardson, S. J., Lauvaux, T., Sarmiento, D. P., Balashov, N. V., Keller, K., Turnbull, J., Gurney, K. R., Liang, J., and Roest, G.: Source decomposition of eddy-covariance CO2 flux measurements for evaluating a high-resolution urban CO2 emissions inventory, Environmental Research Letters, 17, https://doi.org/10.1088/1748-9326/ac7c29, 2022.

Xiao, J.F., Davis, K.J., Urban, N.M., Keller, K.: Uncertainty in model parameters and regional carbon fluxes: A model-data fusion approach. Agricultural and Forest Meteorology, 189-190, 175-186, 2014

Xu, K., S. Metzger, A. R. Desai.: Upscaling tower-observed turbulent exchange at fine spatio-temporal resolution using environmental response functions, Agricultural and Forest Meteorology, 232, 10-22, https://doi.org/10.1016/j.agrformet.2016.07.019, 2017.

Yadav, V., Verhulst, K., Duren, R., Thorpe, A., Kim, J., Keeling, R., Weiss, R., Cusworth, D., Mountain, M., Miller, C., and Whetstone, J.: A declining trend of methane emissions in the Los Angeles basin from 2015 to 2020, Environmental Research Letters, 18, 034004, https://doi.org/10.1088/1748-9326/acb6a9, 2023.

Yi, C., Davis, K. J., Bakwin, P. S., Berger, B. W., and Marr, L. C.: Influence of advection on measurements of the net ecosystem-atmosphere exchange of CO 2 from a very tall tower, Journal of Geophysical Research: Atmospheres, 105, 9991–9999, https://doi.org/10.1029/2000JD900080, 2000